Goal-oriented error estimation for fluid-structure interaction problems

Th. Richter[,a]

[a]*Institute of Applied Mathematics, University of Heidelberg, INF 293/294*
69120 Heidelberg, Germany

Abstract

In this work, we present an adaptive finite element method for the numerical simulation of stationary fluid-structure interaction problems. The coupled system is given in a variational and monolithic Arbitrary Lagrangian Eulerian framework. We derive methods for goal-oriented error estimation and mesh adaptation with the dual weighted residual method. Key to applying this error estimator is the underlying *canonic* variational formulation of the fluid-structure interaction problem by mapping the flow problem to ALE coordinates. The developed method is applied to two and three dimensional stationary benchmark problems coupling the incompressible Navier-Stokes equations with a nonlinear hyper-elastic material law.

Key words: fluid-structure interaction, dual weighted residuals, goal-oriented error estimation, adaptive finite elements, ALE
2010 MSC: 65N30, 74F10

1. Introduction

Topic of this work is an adaptive finite element formulation for coupled fluid-structure interaction (FSI) problems. Fluid structure interactions are part of various technical problems, traditional applications are found in aerodynamics (the elastic behavior of the wing), or in hemodynamics (flow in elastic blood vessels, flow in the moving heart valves). These problems have in common, that complicated three dimensional flow- and structure-domains are coupled, that these domains are moving (the bending of the wing or the contraction of the heart) and in particular, that the coupling between fluid and solid is two-way: the aerodynamic forces bend the wing, the deformation of the aircraft causes new aerodynamic properties. The proper modeling of this coupling is the characteristic difficulty of fluid-structure interaction simulations. In this work we focus on two and three-dimensional stationary problems, where the incom-

---

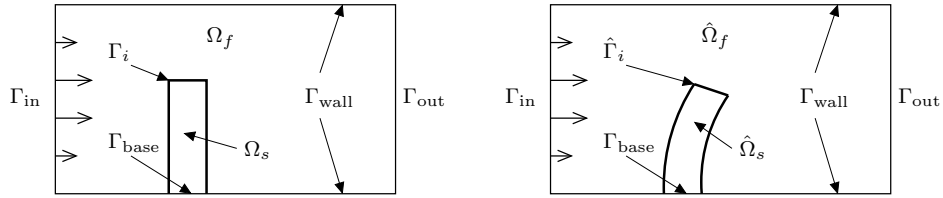*Email address:* `thomas.richter@iwr.uni-heidelberg.de` (Th. Richter)

Figure 1: Typical configuration for a fsi-problem: flow around an elastic obstacle that is attached to the wall at Γ_{base}. Left: reference domain, right: configuration under load.

pressible Navier-Stokes equations are coupled with a hyper-elastic material. A typical, two dimensional configuration is depicted in Figure 1.

For modeling FSI-problems, two coordinate frameworks must be combined: the fixed and particle-centered Lagrangian viewpoint of structure mechanics with the Eulerian spatially centered viewpoint of fluid-mechanics. In FSI applications, the interaction of flow and structure leads to a deformation of the domains, under load, the reference configuration $\Omega = \Omega_f \cup \Omega_s$ will transform in to a new configuration $\Omega = \hat{\Omega}_f \cup \hat{\Omega}_s$, see Figure 1. This new configuration is an unknown part of the solution. Traditionally, so called *partitioned approaches* were considered to separately model and approximate both subproblems while the coupling is realized by an outer iteration. Lately, mainly by progress in computer power, *monolithic models* have been taken into account, to describe the complete coupled system. One well-established monolithic model for FSI-problems are the *Arbitrary Lagrangian Eulerian* (ALE) coordinates, where the flow-problem is mapped onto a fixed reference domain, which is aligned to the also fixed solid domain, see [23, 51, 55, 38, 4, 37]. This approach will be used within this work. Having a common coordinate framework with fixed domains Ω_s and Ω_f at hand will prove to be essential for deriving the adaptive finite element formulation.

In ALE formulation, the FSI problem is given as a complex nonlinear system of partial differential equations. A numerical simulation, in particular considering three dimensional problems is very costly. By using locally refined meshes based on a posteriori error estimation, this effort can be significantly reduced. For optimal efficiency, we will consider a posteriori error estimates which aim at estimating the error in certain *functional outputs*, which are of interest in technical applications. Examples for such functionals are drag- and lift-coefficients in aerodynamics or bending moments in structure dynamics. Functional- or *goal-oriented* error estimates rely on sensitivity information which are given as solutions to *adjoint problems*. The use of sensitivity techniques in error estimation starts with ideas of Babuška and Miller [1, 2] for enhancing the functional-accuracy by post-processing. First work on a posteriori error estimation with help of a duality technique has been done by Eriksson, Johnson and co-workers, see [27, 28, 29, 30, 31] or the survey [26] for details. Becker & Rannacher [8, 9]

further developed this approach into a computation-based method, the *Dual Weighted Residual*-method (DWR), where the sensitivities are approximated as discretized adjoints. Applications to flow and structure problems, are described in the survey [10]. Further works on goal-oriented adaptivity and duality techniques for partial differential equations are found by Giles & Süli [39], Paraschivoiu & Patera [59] or Oden & Prudhomme [58].

While adaptive finite element methods relying on sensitivity information have a long tradition and are well established for flow [10, 17, 41] and structural [60] problems, the consideration of multi-physics problems is a recent development. While the extension to reactive-flows [15, 18] or coupled flow-transport processes [54, 11] is straightforward, an extension to fluid-structure interactions is challenging due to the different coordinate frameworks involved for modeling the two subsystems. It shows, that obtaining adjoint sensitivity information with a proper transport of information through the fluid-structure interface is the major problem. Assuming, that the solution $U \in V$ of the coupled system is described by a variational formulation

$$U \in V: \quad A(U)(\Phi) = F(\Phi) \quad \forall \Phi \in V, \tag{1}$$

the adjoint solution $Z \in V$ is then given as the linearized adjoint with respect to the goal-functional $J : V \to \mathbb{R}$:

$$Z \in V: \quad A'(U)(\Phi, Z) = J'(U)(\Phi) \quad \forall \Phi \in V. \tag{2}$$

By $A'(U)(\cdot, \cdot)$ and $J'(U)(\cdot)$ we denote the Gateaux derivative of $A(\cdot)(\cdot)$ and $J(\cdot)$, respectively. Following the concepts of Becker & Rannacher [10], the error in the goal functional $J(U) - J(U_h)$ is then given in terms of residual information:

$$
\begin{aligned}
J(U) - J(U_h) = {} & \frac{1}{2} \min_{\Phi_h \in V_h} \left\{ F(Z - \Phi_h) - A(U_h)(Z - \Phi_h) \right\} \\
& + \frac{1}{2} \min_{\Phi_h \in V_h} \left\{ J'(U_h)(U - \Phi_h) - A'(U_h)(U - \Phi_h, Z_h) \right\} + \mathcal{R},
\end{aligned}
\tag{3}
$$

with a higher order remainder $\mathcal{R}$.

The problem with applying sensitivity based error estimation to fluid-structure interactions is the lack of a standard variational formulation like (1) which describes the coupled problem. This is mainly due to the fact, that in fluid-structure interaction problems the domain itself is deforming and thus an unknown part in the equation. The fluid domain is depending on the unknown solution itself and has a free-surface character. As the domain is unknown and depending on the solution, so does the functional space $V = V(U)$. And with solution-dependent functional spaces, a linearized adjoint like (2) is not at hand.

Duality techniques for one way coupled problems, where there is no feed-back from the structural- to the flow-problem, are analyzed by Larson and coworkers [54, 11] or Estep an coworkers [32]. Here, sensitivities describe the error propagation between the two subproblems in the coupled setting. The analysis

is however simplified since the coupling is one-way and in particular no free-surface character of the fluid-problem is given. Grätsch & Bathe [40] employ sensitivity based error estimation for fluid-structure interactions by approximating the linearized adjoints (2) with help of finite difference approximations. Dunne and coworkers [24, 25] derived an adaptive finite element scheme for a novel *Fully Eulerian* monolithic formulation. Here, however the underlying variational formulation is not fully consistent, since the coupling conditions are not exactly represented.

It turns out, that the main difficulty with deriving exact linearizations of fluid-structure interactions are the shape-derivatives calculus [63] which allude to the movement of the fluid-domain. Fernández & Moubachir [34] use shape-derivatives to evaluate the Jacobian used in a Newton's method for solving the nonlinear problems. In the context of ALE-coordinates, these shape-derivative appear as derivatives with respect to the domain mapping. A very comprehensive analysis of adjoint formulations for free-surface and coupled fluid-structure interaction problems is given by Brummelen, van der Zee and coworkers. First, they derive sensitivity information for free boundary problems using different adjoint formulations one employing the shape-differential calculus [72] and by differentiating the ALE domain map [73]. These formulations are applied to fluid-structure interactions with string-type structures and linear flow models [71, 35, 70].

After a short collection of notations used in this paper (Section 2) we develop a canonic variational formulation for the coupled fluid-structure interaction problem (Section 3) that fits into the frame of (1). Section 4 is devoted to the stabilized finite element discretization used to approximate the fluid-structure interaction problem and to solution methods for the discretized equations. In Section 5 the DWR-method is presented on the basis of the described variational formulation. In Section 6 numerical examples will elaborate on the performance of the derived error estimator. Finally, in the appendix, we give details on the linearization of the variational formulation.

2. Basic notations

By $\Omega \subset \mathbb{R}^d$ with $d = 2, 3$ we denote a domain. This domain is split into a fluid-part Ω_f and into a solid part Ω_s, each domains in $\mathbb{R}^d$. It holds $\Omega_f \cap \Omega_s = \emptyset$ and $\hat{\Omega} = \bar{\Omega}_f \cup \bar{\Omega}_s$. By $\Gamma_i := \bar{\Omega}_f \cap \bar{\Omega}_s$ we denote the *interface*. In Ω_f the incompressible Navier-Stokes equations are given for the fluid's velocity $v_f : \Omega_f \to \mathbb{R}^d$ and pressure $p_f : \Omega_f \to \mathbb{R}$. In Ω_s an elastic material law is given to describe the solid's deformation $u_s : \Omega_s \to \mathbb{R}^d$. Figure 1 shows a typical configuration of a fsi-problem, where the flow encloses an elastic obstacle. The big challenge of fluid-structure interaction is the deformation of the domains Ω_f and Ω_s under load: the fluid's forces on the obstacle will cause a deformation u_s of the solid via $T_s := \mathrm{id} + u_s : \Omega_s \to \hat{\Omega}_s$. Consequently, the flow domain will move along $\Omega_f \to \hat{\Omega}_f$. When considering stationary problems, a new balance will be given by the loaded configuration $\hat{\Omega} = \hat{\Omega}_f \cup \hat{\Omega}_s$. The layout of this new

configuration is not known, instead it must be considered as unknown part of the solution.

On Ω we define by $L^2(\Omega)$ the Lebesgue space of square integrable functions on Ω with the L^2-inner product and norm:

$$v, w \in L^2(\Omega): \quad (v,w)_\Omega := \int_\Omega vw \, \mathrm{d}x, \quad \|v\|_\Omega := (v,v)_\Omega^{\frac{1}{2}}.$$

Usually, we skip the index Ω when referring to the whole domain and simply use $(\cdot, \cdot)_x := (\cdot, \cdot)_{\Omega_x}$ with $x = s, f$ when referring to one of the subdomains. Further, by

$$\langle v, w \rangle_\Gamma := \int_\Gamma vw \, \mathrm{d}s,$$

we denote the L^2-inner product along (parts of) the boundary. On the interface Γ_i we use for abbreviation the notation $\langle \cdot, \cdot \rangle_i := \langle \cdot, \cdot \rangle_{\Gamma_i}$. By $H^1(\Omega)$ we denote the space of $L^2(\Omega)$-functions with weak derivatives in $L^2(\Omega)$. Finally, by $H_0^1(\Omega; \Gamma)$ we denote the space of $H^1(\Omega)$-functions which have trace zero on (parts of) the boundary $\Gamma \subset \partial\Omega$.

Throughout this work we have to distinguish two different coordinate systems, the undeformed Lagrangian reference system with domain Ω_f and Ω_s and the deformed Eulerian loaded configuration $\hat{\Omega}_f, \hat{\Omega}_s$. All entities, like coordinates $\hat{x}$, derivatives $\hat{\nabla}$ or functions $\hat{v}$ appearing in the Eulerian framework are marked by a hat "ˆ".

3. Problem setting and variational formulations

In this section, a variational formulation for the coupled fluid-structure interaction problem is derived. We start by describing the governing equations used to model the two subfields, fluid and structure.

3.1. The subfield-problems

In the (unknown) fluid domain $\hat{\Omega}_f$ we consider the incompressible Navier-Stokes equations in the standard variational formulation:

Problem 1 (Navier-Stokes, classical formulation)**.** *Given an extension of the Dirichlet profile* $\tilde{v}_{in} \in H^1(\hat{\Omega}_f)^d$ *on* Γ_{in} *and a volume force* $f_f \in L^2(\Omega_f)^d$, *find pressure* $\hat{p}_f$ *and velocity* $\hat{v}_f$

$$\hat{v}_f \in \tilde{v}_{in} + \hat{V}_f, \quad \hat{V}_f := H_0^1(\hat{\Omega}_f; \Gamma_{in} \cup \Gamma_{wall} \cup \hat{\Gamma}_i)^d, \quad \hat{p}_f \in \hat{L}_f := L^2(\hat{\Omega}_f),$$

such that:

$$\hat{A}_f(\hat{v}_f, \hat{p}_f)(\hat{\phi}_f, \hat{\xi}_f) = (\rho_f \hat{f}_f, \hat{\phi}_f)_{\hat{f}} \quad \forall \{\hat{\phi}_f, \hat{\xi}_f\} \in \hat{V}_f \times \hat{L}_f. \tag{4}$$

The semilinear-form $\hat{A}(\cdot)(\cdot)$ *is given as*

$$\hat{A}(\hat{v}_f, \hat{p}_f)(\hat{\phi}_f, \hat{\xi}_f) := (\hat{\sigma}_f, \hat{\nabla}\hat{\phi}_f)_{\hat{f}} + \rho_f(\hat{v}_f \cdot \hat{\nabla}\hat{v}_f, \hat{\phi}_f)_{\hat{f}} + (\hat{\nabla} \cdot \hat{v}_f, \hat{\xi}_f)_{\hat{f}}$$
$$- \rho_f \nu_f \langle \hat{\nabla}\hat{v}_f^T \hat{n}, \hat{\phi}_f \rangle_{\Gamma_{out}}.$$

By ρ_f we denote the fluid's density, by ν_f its kinematic viscosity and by $\hat{\sigma}_f$ the Cauchy-stress tensor

$$\hat{\sigma}_f := \rho_f \nu_f (\hat{\nabla}\hat{v}_f + \hat{\nabla}\hat{v}_f^T) - \hat{p}_f I.$$

Considering viscous fluids we enforce no-slip conditions on the outer wall Γ_{wall} and on the interface boundary $\hat{\Gamma}_i$. Since we deal with the stationary limit only, $\hat{v}_{\hat{\Gamma}_i} = 0$ is used throughout this work.

Remark 1 (Outflow boundary condition). *The additional boundary term on Γ_{out} is added to comply with the* do-nothing condition *[44] used in computational fluid dynamics:*

$$\rho_f \nu_f \hat{\nabla}\hat{v}_f - \hat{p}_f \hat{n} = 0$$

This condition brings along the hidden boundary condition *$\int_{\Gamma_{out}} \hat{p}_f \, d\hat{x} = 0$. Hence, whenever a free outflow boundary is given in the domain, there is no need to filter the constants from the pressure space $\hat{L}_f$. Again, see [44]. The author is aware, that by adding additional boundary integrals to $A_f(\cdot)(\cdot)$ in (4), loss of coercivity leads to an ill-posed problem. However by removing $\rho_f \nu_f \nabla v^T n$ on the outflow boundary, we allow parallel flow profiles to pass the boundary without unphysical deflection that would occur when using the full symmetric tensor.*

The solid problem is governed by a nonlinear elastic material of St. Venant Kirchhoff type [45] in Lagrangian formulation on the reference domain Ω_s:

Problem 2 (St. Venant Kirchhoff material). *Given a volume force $f_s \in L^2(\Omega_s)^d$ and interface-stresses $g_\Gamma \in H^{-1/2}(\Gamma_i)^d$, find the deformation u_s*

$$u_s \in V_s := H_0^1(\Omega_s; \Gamma_{base})^d,$$

such that

$$A_s(u_s)(\phi_s) = (\rho_s f_s, \phi_s)_s + \langle g_\Gamma, \phi_s \rangle_{\Gamma_i} \quad \forall \phi_s \in V_s,$$

where by $A_s(\cdot)(\cdot)$ we denote the semilinear-form

$$A_s(u_s)(\phi_s) := (F_s \Sigma_s, \nabla \phi_s)_s.$$

By ρ_s we denote the solid's density, by $F_s := I + \nabla u_s$ the deformation gradient, by $J_s := \det(F_s)$ its determinant, and finally by Σ_s the second Piola Kirchhoff stress tensor. For a St. Venant Kirchhoff material it holds:

$$\Sigma_s := \lambda_s \operatorname{tr}(E_s) I + 2\mu_s E_s,$$

with the Green-Lagrange strain tensor $E_s := \frac{1}{2}(F_s^T F_s^{-1} - I)$ and λ_s and μ_s being the Lamé coefficient and the shear modulus.

On the outer boundary Γ_{base} we prescribe (for simplicity) a homogenous Dirichlet condition for the displacement of the solid. On the interface Γ_i to the fluid domain, the problem is driven by a Neumann condition.

Coupling of these two problems is by means of prescribing boundary conditions on the common interface Γ_i: first we require continuity of the velocities, which in the stationary limit is already included in the boundary condition $\hat{v}_f = 0$ on $\hat{\Gamma}_i$. Second, we require continuity of the normal-stresses on the interface:

$$F_s(x)\Sigma_s(x)n(x) = \hat{\sigma}_f(\hat{x})\hat{n}(\hat{x}), \quad \text{for } \hat{x} = x + u_s(x) \in \hat{\Gamma}_i.$$

Here, by $x \in \Gamma_i$ and $\hat{x} \in \hat{\Gamma}_i$ we denote *one* point on the interface, once in reference coordinates, once in the deformed coordinate system.

In the following, we combine the interface conditions and the two variational formulations for fluid and structure to one coupled variational problem. We closely follow Ghattas & Li [38] (see [4, 67] for more references). The continuity of fluid's and structure's velocity is naturally given by restricting the velocities trial-spaces trace to zero on $\hat{\Gamma}_i$ as already done so in Problem 1 by using $v_{\hat{\Gamma}_i} = 0$.

The dynamic condition couples the stresses of the fluid and the solid. We employ continuity of these fluxes by relaxing the interface boundary condition for $\hat{\phi}_f \in \hat{V}_f$ in Problem 1. Instead of zero trace, we enforce continuity of the test-functions $\hat{\phi}_f$ and ϕ_s at Γ_i and $\hat{\Gamma}_i$, respectively. By this *variationally consistent load evaluation* [38, 33, 21, 55] the proper coupling condition appears with integration by parts at the interface. We combine the test-spaces to satisfy:

$$\hat{\phi}_f(\hat{x}) = \phi_s(x) \text{ for } \hat{\Gamma}_i \ni \hat{x} \xleftarrow{\text{id}+u_s} x \in \Gamma_i,$$

by summing up the semi-linear forms A_f and A_s integration by parts results in the classic formulation of the two sub-problems as well as the boundary contribution on Γ_i and $\hat{\Gamma}_i$, respectively:

$$\int_{\hat{\Gamma}_i} \hat{\sigma}_f \hat{n}_f \cdot \hat{\phi}_f(\hat{x}) \, d\hat{x} + \int_{\Gamma_i} F_s \Sigma_s n_s \cdot \phi_s(x) \, dx = 0.$$

Note that for the Cauchy stress tensor σ_s transformed to Eulerian coordinates [45] (then denoted by $\hat{\sigma}_s$) it holds

$$F_s \Sigma_s = J_s \sigma_s F_s^{-T} \;\Rightarrow\; (F_s \Sigma_s)(x)n_s(x) = (J_s \sigma_s F_s^{-T})(x)n(x) = \hat{\sigma}_s(\hat{x})\hat{n}(\hat{x}). \quad (5)$$

Problem 3 (Coupled problem, variational formulation). *Find*

$$\hat{v}_f \in \tilde{v}_{in} + \hat{V}_f, \; \hat{p}_f \in \hat{L}_f, \; u_s \in V_s,$$

such that

$$\hat{A}_f(\hat{v}_f, \hat{p}_f)(\hat{\phi}_f, \hat{\xi}_f) + A_s(u_s)(\phi_s) = (\rho_f f_f, \hat{\phi}_f)_{\hat{f}} + (\rho_s f_s, \phi_s)_s$$

for all $\{\hat{\phi}_f, \phi_s\} \in \hat{V}_{fs}$, $\hat{\xi}_f \in \hat{L}_f$, where the combined test-space $\hat{V}_{fs}$ is defined as

$$\hat{V}_{fs} := \left\{ \{\hat{\phi}_f, \phi_s\} \in [H_0^1(\hat{\Omega}_f; \Gamma_{in} \cup \Gamma_{wall})]^d \times V_s, \; \hat{\phi}_f(x + u_s(x)) = \phi_s(x) \right\}.$$

7

Remark 2. *The function space $\hat{V}_{fs}$ used to define the variational formulation in Problem 3 depends on the solution u_s itself. This somewhat awkward setting is not a strict Galerkin formulation. The dual weighted residual method cannot be immediately applied in its canonic setting as presented in the introduction.*

It is far from trivial to derive exact linearized adjoints based on this variational formulation since derivatives with respect to the interface coupling in the test-space $\hat{V}_{fs}$ must be incorporated. In the context of shape- or topology-optimization *the* shape-derivatives *[63] play an important role. Fernández & Moubachir [34] use shape calculus to obtain exact Jacobians for fluid-structure interactions. Van der Zee and coworkers [72, 73] accurately analyze adjoints for linear problems including this typical free surface character using different techniques.*

In the following section we will further modify the variational formulation by mapping the flow problem onto ALE coordinates. This mapping is applied on the continuous level leading to a canonic variational formulation. Deriving linearized adjoints is then accomplished by standard techniques. This procedure is similar to the domain-map linearization approach discussed by van der Zee and coworkers [72].

3.2. A canonical variational formulation of the coupled problem

The difficulty of the variational Problem 3 lies in the dependency of the functional spaces on the solution itself. We "hide" this dependency by mapping the flow problem onto a fixed reference domain Ω_f via a transformation,

$$\mathcal{A}_f : \Omega_f \to \hat{\Omega}_f, \tag{6}$$

and by defining the fluid's velocity and pressure onto this reference domain

$$v_f(x) := \hat{v}_f(\hat{x}) = \hat{v}_f(\mathcal{A}_f(x)), \quad p_f(x) := \hat{p}_f(\hat{x}) = \hat{p}_f(\mathcal{A}_f(x)).$$

These *Arbitrary Eulerian Lagrangian* coordinates have been widely used to model free-surface problems [51, 48] as well as fluid-structure interactions, see for instance [55, 4, 42, 37, 19, 20] among many other contributions.

Given sufficient regularity of the mapping $\mathcal{A}_f$ the variational formulation of the Navier-Stokes equations can be expressed on the reference coordinate system. By standard transformation of integrals and derivatives, Problem 1 turns to (see e.g. [36, 55] for details on this transformation)

Problem 4 (Navier-Stokes in ALE coordinates, variational setting)**.** *Find*

$$v_f \in \tilde{v}_{in} + V_f, \ V_f := H_0^1(\Omega_f; \Gamma_{in} \cup \Gamma_{wall} \cup \Gamma_i), \ p_f \in L_f := L^2(\Omega_f),$$

such that

$$A_f(v_f, p_f)(\phi_f, \xi_f) = (J\rho_f f_f, \phi_f)_f, \quad \forall\{\phi_f, \xi_f\} \in V_f \times L_f,$$

where the transformed semi-linear form $A_f(\cdot)(\cdot)$ is defined by

$$A_f(v_f, p_f)(\phi_f, \xi_f) := (J_f \sigma_f F_f^{-T}, \nabla \phi_f)_f + \rho_f (J_f F_f^{-1} v_f \cdot \nabla v_f, \phi_f)_f$$
$$+ (\nabla \cdot (J_f F_f^{-1} v_f), \xi_f)_f - \rho_f \nu_f \langle J_f F_f^{-T} \nabla v_f^T F_f^{-T} n_f, \phi_f \rangle_{\Gamma_{out}}$$

with the fluid' stress tensor transformed to the artificial ALE coordinate system

$$\sigma_f = \rho_f \nu_f (\nabla v_f F_f^{-1} + F_f^{-T} \nabla v_f^T) - p_f I,$$

and with the gradient of the ALE mapping and its determinant

$$F_f := \nabla \mathcal{A}_f, \quad J_f := \det(F_f).$$

Remark 3. *If the mapping $\mathcal{A}_f : \Omega_f \to \hat{\Omega}_f$ would be given a priori, Problem 4 is in a standard setting, function spaces and domains do not depend on the unknown solution any more. Further, the semi-linear-forms of Problems 4 and 2 are defined on matching domain and share a common interface $\Gamma_i = \bar{\Omega}_f \cap \bar{\Omega}_s$. The dynamic coupling condition in Problem 3 simply turns to (see (5)):*

$$\langle J_f \sigma_f F_f^{-T} n_f, \phi_f \rangle_{\Gamma_i} + \langle J_s \sigma_s F_s^{-T} n_s, \phi_s \rangle_{\Gamma_i} = 0$$

Removing the domain's dependency on the solution comes at the price of a highly nonlinear system of equations for the fluid problem and the introduction of an additional unknown, the ALE-mapping $\mathcal{A}_f$. We construct this mapping by introducing an artificial deformation u_f of the fluid-domain $\mathcal{A}_f(x) = x + u_f(x)$. Finding this deformation u_f is usually referred to as the "mesh motion problem". At the boundaries of the fluid domain Ω_f, Dirichlet conditions must be satisfied to guarantee that $\mathcal{A}_f$ is a one-to-one correspondence between the domains Ω_f and $\hat{\Omega}_f$:

$$u_f = u_s \text{ on } \partial\Gamma_i, \quad u_f = 0 \text{ on } \partial\Omega_f \setminus \Gamma_i.$$

The condition on the interface Γ_i assures, that $\mathcal{A}_f(\Gamma_i) = \hat{\Gamma}_i$. On the outer boundaries $\Omega_f \setminus \Gamma_i$ the condition could be relaxed to a slip-condition $u_f \cdot n = 0$ [68]. In the interior of the fluid-domain a differential operator (satisfying a maximum principle) is used to define u_f.

Problem 5 (Mesh motion problem). *Given an extension of the interface deformation $u_{\Gamma_i} = u_s|_{\Gamma_i}$ into the fluid domain $\tilde{u}_s \in H^1(\Omega_f)^d$, find*

$$u_f \in \tilde{u}_s + W_f, \quad W_f := H_0^1(\Omega_f; \partial\Omega_f)^d,$$

such that

$$A_m(u_f)(\psi_f) = 0 \quad \forall \psi_f \in W_f, \quad A_m(u_f)(\psi_f) := (\sigma_m, \nabla \psi_f)_f,$$

with the Cauchy stress tensor of a pseudo-elastic material:

$$\sigma_m = \lambda_m \operatorname{div}(u_f) I + \mu_m (\nabla u_f + \nabla u_f^T).$$

Remark 4 (ALE mapping). *Sufficient regularity of the ALE mapping is necessary to guarantee invariance of the Sobolew-spaces under coordinate transformation*

$$H^1(\Omega_f) \approx H^1(\hat{\Omega}_f).$$

Classical analysis [69] ask for $\mathcal{A}_f$ being a C^1-diffeomorphism. Nobile [36] relaxes this assumption to requiring $\mathcal{A}_f, \mathcal{A}_f^{-1} \in W^{1,\infty}$ in the context of fluid-structure interaction.

The linear elasticity equation used in Problem 5 is known not to satisfy this regularity, if the domain Ω_f has obtuse interior angles, which is usually the case in the context of fluid-structure interaction where some solid is embedded in the fluid-domain. To always guarantee sufficient regularity of the mapping $\mathcal{A}_f$, one can use a biharmonic extension to construct u_f. Since in this work we only consider small deformation we successfully work with the pseudo-elastic extension using material parameters μ_m and λ_m in the auxetic regime *or even a simple harmonic extension only. In addition to extensive literature [52, 53, 64] on the analysis of these mesh motion techniques, see [43, 68] for a numerical comparison of various methods.*

The flow field deformation u_f and the solid deformation u_s are continuous at Γ_i. For deriving a monolithic variational formulation of the coupled problem this continuity is embedded into one common trial space $u \in V$ and by denoting the restrictions to the subdomains as $u_f := u|_{\Omega_f}$ and $u_s := u|_{\Omega_s}$, respectively. Likewise, since the test-functions ϕ_f and ϕ_s are continuous on the whole domain Ω and choosing in the globally defined space $\phi \in V'$:

Problem 6 (Coupled problem, canonic variational formulation). *Given the extension of the inflow profile $\tilde{U}_{in} := \{0, \tilde{v}_{in}, 0\}$ find $U := \{u, v, p\}$*

$$U \in \tilde{U}_{in} + X, \ X := V \times V_f \times L_f$$

with

$$V := H_0^1(\Omega; \partial\Omega)^d, \quad V_f := H_0^1(\Omega_f; \partial\Omega_f \setminus \Gamma_{out})^d, \quad L_f := L^2(\Omega_f),$$

such that

$$A(U)(\Phi) = (J_f \rho_f f_f, \phi_f)_f + (\rho_s f_s, \phi_s)_s \quad \forall \Phi \in X' := \{\phi, \psi, \xi\} \in V' \times V_f' \times L_f,$$

with

$$V' := H_0^1(\Omega; \partial\Omega \setminus \Gamma_{out})^d, \quad V_f' := H_0^1(\Omega_f; \partial\Omega_f)^d, \quad L_f := L^2(\Omega_f),$$

and with the combined semi-linear form

$$A(u, v, p)(\phi, \psi, \xi) := A_f(v_f, p)(\phi_f, \xi) + A_s(u_s)(\phi_s) + A_m(u_f)(\psi),$$

defined as in Problem 2, 4 and 5.

Remark 5 (Test & trial spaces). *Test- X' and trial-space X differ, hence Problem 6 is a Petrov-Galerkin formulation. The small difference in the spaces however only appears due to the free outflow condition and vanishes in the case $\Gamma_{out} = \emptyset$. Regarding the interface Γ_i, test- and trial-spaces have the same setup. In context of the important interface coupling the formulation can be considered as a standard Galerkin-approach.*

4. Finite Element Discretization for FSI Problems

For discretization of Problem 6, a stabilized finite element discretization with equal-order finite element for all variables is used. First, let Ω_h be a finite element triangulation of the domain Ω into open quadrilaterals or hexahedrals which fulfills the usual structure- and shape-regularity assumptions relaxed by introducing hanging nodes to allow for local mesh refinement, see [22, 18]. Further, Ω_h must be conforming with the domain partitioning, such that every element $K \in \Omega_h$ is either entirely in the fluid domain Ω_f or in the solid domain Ω_s and it exists a partitioning $\Omega_h = \Omega_{f,h} \cup \Omega_{s,h}$. Finally, every mesh is supposed to have a *patch structure*: every element $K \in \Omega_h$ is part of 2^d elements arising from the same element by uniform refinement. This patch-structure is used for both the stabilization technique and the error estimator. Again see [18]. On Ω_h we denote by $V_h^{(r)}(\Omega_h; \Gamma)$ the usual space of isoparametric finite element functions of degree r with trace zero on Γ. Then, the discrete solution $U_h := \{u_h, v_h, p_h\}$ is found in the discrete space $X_h \subset X$:

$$X_h := [V_h^{(r)}(\Omega_h; \partial\Omega)]^d \times [V_h^{(r)}(\Omega_{f,h}; \partial\Omega_f \setminus \Gamma_{\text{out}})]^d \times V_h^{(r)}(\Omega_{f,h}). \qquad (7)$$

The test-space $X_h' \subset X'$ is defined likewise with the already mentioned modifications to comply with the outflow condition:

$$X_h' := [V_h^{(r)}(\Omega_h; \partial\Omega \setminus \Gamma_{\text{out}})]^d \times [V_h^{(r)}(\Omega_{f,h}; \partial\Omega_f)]^d \times V_h^{(r)}(\Omega_{f,h}). \qquad (8)$$

Using these spaces, the discrete Petrov-Galerkin formulation is given by restriction to the subspaces $X_h \subset X$ and $X_h' \subset X'$.

4.1. Local projection stabilization

The incompressible Navier-Stokes system as basis of the fluid-structure interaction problem asks for approximation spaces fulfilling the inf-sup condition. The equal-order space X_h is not inf-sup stable, hence a modification of the semi-linear form $A(\cdot)(\cdot)$ is necessary. Further, the transport term asks for additional stabilization if the flow gets convection dominated. While the well established PSPG/SUPG method by Hughes, Franca and Balestra [50] and Hughes and Brooks [49] is applicable also for fluid-structure interaction problems, see Wall [67], we refrain from using it due to the high numerical effort and the artificial coupling terms introduced by ensuring a consistent formulation. Instead, we employ the *Local Projection Stabilization method* (LPS) as introduced by Becker

and Braack [5, 6] both for stabilizing the *inf-sup* condition and dominant convective terms. However, since the stationary problems regarded in this work do not exhibit strong convective regimes we focus on the pressure stabilization.

Here, fluctuations of the pressure $\kappa_H(p_h) := p_h - \pi_H p_h$ with regard to a coarser space X_H with inf-sup stable velocity-pressure pairing $[V_h^{(r)}]^d - Q_H$ are added. For higher order finite elements $r \geq 2$ we choose a Taylor-Hood element with $Q_H := V_h^{(r-1)}(\Omega_{f,h})$ as inf-sup stable as stable basis. In the case $r = 1$ a variant of the Taylor-Hood element is chosen, where the stable pressure space is of the same order, but defined on a mesh with double mesh-size $Q_H := V_{2h}^{(r)}$. Due to the patch-structured mesh, these two projection operators $\pi_H : V_h^{(r)} \to Q_H$ are easily evaluated by a local replacement of the basis functions, since the nodal bases of $V_h^{(r)}$ and Q_H share the same supporting points. See [5, 18, 16] for details.

Problem 7 (Stabilized fluid-structure interaction problem). *Given a discrete extension of the Dirichlet data $\tilde{U}_{h,in}$, find $U_h \in \tilde{U}_{h,in} + X_h$ such that*

$$A_h(U_h)(\Phi_h) := A(U_h)(\Phi_h) + S_h(U_h)(\Phi_h) = F(\Phi_h) \quad \forall \Phi_h \in X_h',$$

with the stabilization form

$$S_h(U_h)(\Phi_h) := \sum_{K \in \Omega_{f,h}} (\alpha_K \tilde{J} \tilde{F}^{-1} \nabla \kappa_H(p_h), \tilde{F}^{-1} \nabla \kappa_H(\xi_h))_K$$

where X_h and X_h' are defined by (7) and (8), respectively, and with the fluctuation operator $\kappa_H := \mathrm{id} - \pi_H$. The stabilization parameter is chosen as $\alpha_K = \alpha_0 h_K^2 (\rho_f \nu_f + \rho_f h_K \|\tilde{v}_h\|_{\infty,K})^{-1}$

4.2. Solution scheme

Problem 7 is a highly nonlinear complex system of partial differential equations. We iteratively solve these equations by a simplified Newton method. Given an initial value $U_h^{(0)} \in U_h^D + X_h$ we solve for the update $W_h^{(t)} \in X_h$ with $U_h^{(t+1)} = U_h^{(t)} + W_h^{(t)}$ as solution of the linear system:

$$A_h'(U_h^{(t)})(W_h^{(t)}, \Phi_h) = F(\Phi_h) - A_h(U_h^{(t)})(\Phi_h) \quad \forall \Phi_h \in X_h'.$$

The Gateaux-derivative of $A_h(\cdot)(\cdot)$ is formally defined as

$$A_h'(U_h^{(t)})(W_h, \Phi_h) := \frac{d}{ds} A_h(U_h^{(t)} + sW_h)(\Phi_h)\Big|_{s=0}. \tag{9}$$

This derivative is calculated analytically from the definition given in Problems 2, 4, 5 and 7. Details on the calculation of the derivatives are given in the literature [34, 4] and the appendix. In many approaches [56, 57, 65] the Jacobian is approximated by finite differences. But since we anyway need exact linearizations for duality based error estimation, we use exact derivatives for the Jacobian. By $\mathbf{A}_h$, we denote the system matrix defined as (9). It will turn out,

that the adjoint system matrix is – up to a small modification concerning the outflow boundary – given by the transpose of this Jacobian, compare (2). In the appendix we give details on all derivatives appearing in the Jacobian (and the adjoint problem).

Remark 6 (Linearization of the Local Projection Stabilization). *We consider the stabilization form $S_h(\cdot)(\cdot)$ to be bilinear by* freezing *the velocity dependence of the parameters α_K using an approximation $\tilde{v}_f$ and by also freezing the domain transformation at some known approximation $\tilde{J}$ and $\tilde{F}$. Hence, it holds $S_h'(\cdot)(\cdot) = S_h(\cdot)(\cdot)$. Further, $S_h(\cdot)(\cdot)$ is symmetric.*

Every step of the Newton method asks for solving a linear system of equations $\mathbf{A}_h^{(t)}\mathbf{W}_h^{(t)} = \mathbf{B}_h^{(t)}$. The matrix $\mathbf{A}_h^{(t)}$ is very large, ill-conditioned and unsymmetric. For solving, we employ a multigrid-preconditioned GMRES iteration. As smoothing operator, a partitioned iteration with ILU-preconditioning is applied.

5. A posteriori error estimation and mesh refinement

Problem 7 is written in a standard monolithic variational formulation, however using a Petrov-Galerkin approach with slight differences between X and X' at the outflow boundary. Dual weighted error estimation is immediately applicable in terms of (1), (2) and (3). In this section we will first expand the original results of Becker & Rannacher [10] to consider stabilization terms, then, we focus on the realization of goal oriented error estimator for fluid-structure interactions with a detailed discussion of the adjoint problems as well as a discussion of the remainder terms appearing in the process of error estimation.

5.1. The dual weighted residual method

We start by citing the main result, Theorem 2, from [10] with a slight modification to include stabilization terms like the Local Projection Stabilization in Problem 7. Let $J(\cdot)$ be some functional of interest on the space X. We define two Euler-Lagrange functionals on $X \times X'$:

$$
\begin{aligned}
L(U, Z) &:= J(U) + F(Z) - A(U)(Z), \\
L_h(U, Z) &:= J(U) + F(Z) - A_h(U)(Z) = L(U)(Z) - S_h(U)(Z).
\end{aligned}
\tag{10}
$$

The primal solutions $U \in X$ and $U_h \in X_h$, and the adjoint solutions $Z \in X'$ and $Z_h \in X_h'$ are given as stationary points of L and L_h in (10):

$$
\begin{aligned}
L'(U, Z)(\Psi, \Phi) &:= \left\{ J'(U)(\Psi) - A'(U)(\Psi, Z) \right\} \\
&\quad + \left\{ F(\Phi) - A(U)(\Phi) \right\} = 0 \qquad \forall \{\Psi, \Phi\} \in X \times X' \\
L_h'(U_h, Z_h)(\Psi_h, \Phi_h) &:= \left\{ J'(U_h)(\Psi_h) - A_h'(U_h)(\Psi_h, Z_h) \right\} \\
&\quad + \left\{ F(\Phi_h) - A_h(U_h)(\Phi_h) \right\} = 0 \quad \forall \{\Psi_h, \Phi_h\} \in X_h \times X_h'.
\end{aligned}
\tag{11}
$$

13

Let $E_h^U := U - U_h \in X$ and $E_h^Z := Z - Z_h \in X'$.

Theorem 1 (Error representation for the fluid-structure interaction problem). *Let $\{U, Z\} \in X \times X'$ and $\{U_h, Z_h\} \in X_h \times X_h'$ be defined by (11). If $L(\cdot, \cdot)$ is three times differentiable, it holds:*

$$J(U) - J(U_h) = \frac{1}{2} \left\{ J'(U_h)(U - i_h U) - A_h'(U_h)(U - i_h U, Z_h) \right\}$$

$$+ \frac{1}{2} \left\{ F(Z - i_h Z) - A_h(U_h)(Z - i_h Z) \right\} + \frac{1}{2} S_h(U, Z_h) + \frac{1}{2} S_h(U_h, Z) + \mathcal{R}^{(3)}(E_h^U, E_h^Z),$$

$$(12)$$

where $\mathcal{R}^{(3)}$ is a remainder of third order in the errors:

$$\mathcal{R}^{(3)} := \frac{1}{2} \int_0^1 \left\{ J'''(U_h + s E_h^U)(E_h^U, E_h^U, E_h^U) - 3 A''(U_h + s E_h^U)(E_h^U, E_h^U, E_h^Z) \right.$$

$$\left. - A'''(U_h + s E_h^U)(E_h^U, E_h^U, E_h^U, E_h^Z) \right\} s(s-1) \, ds. \quad (13)$$

PROOF: For the two Euler-Lagrange functionals L and L_h it holds by (10):

$$J(U) - J(U_h) = L(U, Z) - L_h(U_h, Z_h) = L(U, Z) - L(U_h, Z_h) + S_h(U_h, Z_h)$$

$$= \int_0^1 \frac{d}{ds} L(U_h + s E_h^U, Z_h + s E_h^Z) ds + S_h(U_h, Z_h)$$

We approximate this integral with the trapezoidal rule, where due to conformity $X_h \times X_h' \subset X \times X'$, the term belonging to $s = 1$ vanishes $L'(U, Z)(E_h^U, E_h^Z) = 0$:

$$J(U) - J(U_h) = \frac{1}{2} L'(U_h, Z_h)(E_h^U, E_h^Z) + S_h(U_h, Z_h) + \mathcal{R}^{(3)}(E_h^U, E_h^Z).$$

Using (11), and Remark 6, the error representation turns to:

$$J(U) - J(U_h) = \frac{1}{2} \left\{ L_h'(U_h, Z_h)(E_h^U, E_h^Z) + S_h(U)(Z_h) + S_h(U_h)(Z) \right\} + \mathcal{R}^{(3)}.$$

$$(14)$$

By using Galerkin-Orthogonality $L_h'(U_h, Z_h)(\Phi_h, \Psi_h) = 0$ for all $\{\Phi_h, \Psi_h\} \in X_h \times X_h'$ we can insert local interpolations operators:

$$J(U) - J(U_h) = \frac{1}{2} \left\{ L_h'(U_h, Z_h)(U - i_h U, Z - i_h Z) + S_h(U)(Z_h) + S_h(U_h)(Z) \right\} + \mathcal{R}^{(3)}.$$

$\square$

Note, that it is not possible to evaluate this error representation as the unknown quantities $U \in X$, $Z \in X'$ and the corresponding interpolations appear. In the following paragraphs we will present approximative techniques for accessing the error estimate. This approximation will be of lesser accuracy than the cubic remainder $\mathcal{R}^{(3)}$.

14

5.2. Application to fluid-structure interactions

Problem 7 is in a canonic form. The discretized adjoint solution $Z_h \in X_h'$ is given as solution of the system (compare (11))

$$Z_h \in X_h' : \quad A_h'(U_h)(\Psi_h, Z_h) = J'(U_h)(\Psi_h) \quad \forall \Psi_h \in X_h.$$

These derivatives can easily be evaluated analytically by tedious application of product rule and chain rule using the definition of $A_f(\cdot)(\cdot)$ and $A_s(\cdot)(\cdot)$ from Problems 2 and 4 in the continuous function spaces X and X'. In the appendix, we will give details on the linearization of the coupled fluid-structure interaction system. Further, since the function spaces X_h and X_h' differ only with regard to the outflow boundary condition, the adjoint system matrix $\mathbf{A}_h^*$ is up to a small modification at these boundaries, the transpose of the Newton-Jacobian $\mathbf{A}_h$.

The quality of the error estimator is considerably controlled by the remainder $\mathcal{R}^{(3)}$ which consists of third derivatives of the Euler-Lagrange functional $L(U, Z)$. In terms of fluid-structure interaction the derivatives with regard to the mesh-motion can be problematic. It holds (see the appendix for details):

$$\frac{\partial^3 F^{-1}(u)}{\partial^3 u}(E_h, E_h, E_h) = -[F^{-1}\nabla E_h]^3 F^{-1}.$$

This term is formally of third order in the error. However, it may get large, if F gets irregular, i.e. in the case $J = \det(F) \to 0$ which is possible for problems where very large deformations are involved. Here, a more sophisticated mesh motion technique, in particular using Jacobian-based stiffening, can help to reduce the influence of the remainder, see [64].

5.3. Error estimation

The error identity still contains the unknown solutions U and Z. First, we need to neglect the remainder terms. This is justifiable, if the regularity of the problem is sufficient. Further, U and Z appear in the interpolation errors as weights for the error identity. In [10] various techniques for approximating the continuous solutions are discussed. Most rely on solving for $U_h^*, Z_h^* \in X_h^*$ using a discrete space with higher resolution. In terms of very complex fluid-structure interaction problems, and in particular in three dimensions, an approximation using a finer space is usually out of bounds. Instead, we will rely on error expansion results which yield a higher order convergence for the errors gradient and which can by used for higher order reconstruction. These results are known e.g. for the Poisson equation or Stokes equations [12, 13], where fourth order node-wise reconstruction is possible on uniform meshes, given sufficient regularity of the solution. We note however, that theoretical results concerning super-approximation for fsi-problems are not available.

In classical application of the dual weighted residual method [8, 7], the error identity is transformed with local integration by parts on every mesh element to recover the strong formulation of the problem and additional jump-terms over the edges. In terms of fluid-structure interactions we will avoid this transformation since the evaluation of the classical formulation is very costly due to the
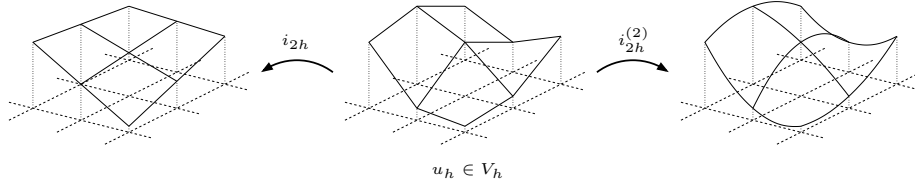
Figure 2: Interpolation of a discrete function $u_h \in V_h$ into higher order space $i_{2h}^{(2)} : V_h \to V_{2h}^{(2)}$ (right) and interpolation into a coarse space $i_{2h} : V_h \to V_{2h}$ (left).

second derivatives and strong nonlinearities evoked by the ALE mapping $\mathcal{A}_f$. Instead we directly approximate the error identity (12) by replacing

$$U - i_h U \approx i_h^* U_h - U_h, \quad Z - i_h Z \approx i_h^* Z_h - Z_h,$$

where $i_h^* : X_h \to X_h^*$ is the interpolation into a space with higher resolution. See Figure 2. Here, we use the space of double polynomial degree on the mesh with double mesh-size $X_h^* = X_{2h}^{(2)}$. This space shares its degrees of freedom with the space X_h and since every mesh is patch-structured (see Section 4), the interpolation can be constructed locally, by simply replacing the basis functions:

$$U_h = \sum_{i=1}^N \mathbf{U}_i \Phi_i \quad \Rightarrow \quad i_{2h}^{(2)} U_h = \sum_{i=1}^N \mathbf{U}_i \Phi_i^{(*)}, \tag{15}$$

where by $\{\Phi_i^{(*)}\}$ we denote the Lagrange nodal basis functions of $X_{2h}^{(2)}$. Note, that $\Phi_i(x_j) = \Phi_i^{(*)}(x_j) = \delta_{ij}$ for all mesh-nodes $x_j \in \Omega_h$. The continuous solution further appears as $i_h U$ and $i_h Z$ in the stabilization parts of the error identity. Since the Local Projection Stabilization consists of local fluctuations only, we can approximate by

$$S_h(U, Z_h) \approx S_h(U_h, Z_h) \approx S_h(U_h, Z).$$

Finally, we estimate the error by

$$\eta_h(U_h, Z_h) := \frac{1}{2} \Big\{ J'(U_h)(i_{2h}^{(2)} U_h - U_h) - A'(U_h)(i_{2h}^{(2)} U_h - U_h, Z_h) \Big\}$$
$$+ \frac{1}{2} \Big\{ F(i_{2h}^{(2)} Z_h - Z_h) - A(U_h)(i_{2h}^{(2)} Z_h - Z_h) \Big\} + S_h(U_h, Z_h). \tag{16}$$

In Section 6, numerical examples will demonstrate the accuracy of this approximation $\eta_h(U_h, Z_h) \approx J(U) - J(U_h)$.

5.4. Localization and error estimation

For practical mesh adaptation purposes, we need to localize the error estimator $\eta_h(U_h, Z_h)$. It is well known [10], that simply restricting the element-wise

contributions of (16) to the elements $K \in \Omega_h$ and taking the absolute values does not yield the proper local order of convergence. Hence, one usually transforms with integration by parts and includes fluxes over the element-edges. As argued before, this is not practical in context of fluid-structure interactions. Here, we follow the concepts introduced in [61, 14] to obtain the correct local order by applying a local filtering operation using once more the patch structure of the meshes.

For localization and error estimation we omit the additional stabilization term $S_h(U_h, Z_h)$. Using the notation $x := \{U, Z\}$ and $x_h := \{U_h, Z_h\}$ we write the residual part of the estimator (16) in compact notation as

$$\eta(x_h) := \mathcal{R}_h(x_h)(x - i_h x),$$

where by $\mathcal{R}_h$ we denote the residual terms of (16). This residual is orthogonal on X_h. Hence a further interpolation $i_{2h} x_h \in X_{2h}$ into the space $X_{2h} \subset X_h$ on a coarse patched mesh may by inserted:

$$\eta(x_h) = \mathcal{R}_h(x_h)((x - i_h x) - i_{2h}(x - i_h x)).$$

See Figure 2 for a sketch of this interpolation operator. Due to the patch-structured mesh, this space is easily accessible, by another exchange of the basis functions similar to (15). Note, that $i_{2h}(x - i_h x) = 0$, but since $i_{2h} i_h = i_h i_{2h}$ it holds

$$\eta(x_h) = \mathcal{R}_h(x_h)((x - i_{2h} x) - i_h(x - i_{2h} x)).$$

Here, we approximate as discussed in Section 5.3 (by

$$\eta(x_h) \approx \mathcal{R}_h(x_h)((i_{2h}^{(2)} x_h - i_{2h} x_h) - i_h(i_{2h}^{(2)} x_h - i_{2h} x_h)).$$

With the notation $\chi_h := (\boldsymbol{\chi}_i)_i$ and $\boldsymbol{\chi}_i := \mathcal{R}_h(x_h)(\Phi_i^{(*)} - \Phi_i)$ it holds:

$$\eta_h(x_h) := \sum_{i=1}^{N} \eta_i, \quad \eta_i := (\chi_h - i_{2h}\chi_h)_i.$$

The error indicators η_i are defined as nodal values. For every $x_i \in \Omega_h$ on the corner of a patch it holds $\eta_i = 0$. Evaluating the error estimator and the error indicators asks for two residual integrations, once with test-functions of higher order. Localization is performed by transformations on the algebraic level only.

Mesh adaptation is driven by an easy balancing condition. We refine those mesh nodes that have an indicator value above the average:

$$\text{refine node } x_i, \text{ if } |\eta_i| \geq \frac{\alpha}{N} \sum_{j=1}^{N} |\eta_j|, \tag{17}$$

with $\alpha \approx 1$. Refining a node x_i means refining the adjacent elements. If a hanging node is to be refined, we only refine the coarser element. For problems with strong gradients (e.g. at reentrant edges) we choose $\alpha > 1$ for a sharper refinement.
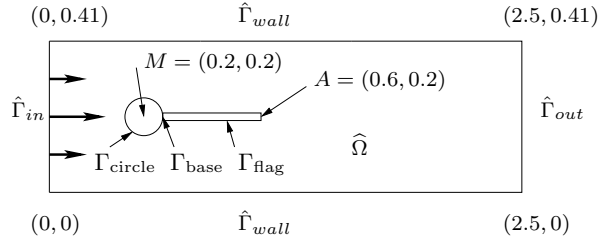
17

Figure 3: Flow around cylinder with elastic beam with circle-center $M = (0.2, 0.2)$ and radius $r = 0.05$.

6. Numerical Results

In this section, we study two problems and show the efficiency of the dual weighted residual method. First we consider the stationary FSI-1 benchmark as proposed by Hron, Turek et. al. in [47]. In this two-dimensional problem, a laminar flow around a circular obstacle with an attached elastic beam is considered, see Figure 8. Quantity of interest is the drag coefficient of the obstacle as well as the deformation of the tip of the beam.

Secondly, as a three-dimensional benchmark problem, the laminar flow over an elastic obstacle mounted on the wall is considered. As quantities of interest we again evaluate the deformation in a point within the elastic structure and the drag coefficient of the obstacle.

6.1. The FSI-1 benchmark problem

First, we consider the stationary benchmark problem FSI-1 [19, 20]. Here, the laminar flow around a cylinder, with an attached elastic beam is simulated. Figure 3 shows a sketch of the configuration.

Problem configuration. Three benchmark problems have been proposed by Hron & Turek [47]. We limit the considerations to the stationary FSI-1 test-case. The flow is laminar with Reynolds-number $Re = 20$ and driven by a parabolic inflow profile with average velocity $\bar{v}_f = 0.2$. For the structural problem, the St. Venant-Kirchhoff material law is used in a slightly compressible setting with Poisson ratio $\nu_s = 0.4$:

$$\rho_f = \rho_s = 1000, \quad \nu_f = 10^{-3}, \quad \mu_s = 5 \cdot 10^5, \quad \lambda_s = 2 \cdot 10^6, \quad \bar{v}_f = 0.2$$

As quantities of interest, we measure the horizontal and vertical deflection of the structure in the point $A = (0.6, 0.2)$ on the tip of the beam, as well as the drag- and lift- coefficient of the complete obstacle (including rigid circle and the elastic beam):

$$
\begin{aligned}
J_{\mathrm{drag}}(U) &:= \int_S (J\sigma_f F^{-T})n_f \cdot e_1 \, \mathrm{d}s & J_{\mathrm{lift}}(U) &:= \int_S (J\sigma_f F^{-T})n_f \cdot e_2 \, \mathrm{d}s \\
J_{\mathrm{x}}(U) &:= u_1(A) & J_{\mathrm{y}}(U) &:= u_2(A),
\end{aligned}
$$

where $e_i := (\delta_{i1}, \delta_{i2})$ are the Cartesian unit vectors and $S := \Gamma_{\mathrm{flag}} \cup (\Gamma_{\mathrm{circle}} \setminus \Gamma_{\mathrm{base}})$.

18

Evaluation of the surface integral. For easier evaluation, we modify the functional expression. Let Γ_{circle} be the boundary, $\Gamma_{\mathrm{base}} \subset \Gamma_{\mathrm{circle}}$ that part of the circle, where the solid domain Ω_s is attached. Then, by using the dynamic coupling condition on Γ_i it holds:

$$J_{\mathrm{drag}}(U) = \int_{\Gamma_{\mathrm{circle}} \backslash \Gamma_{\mathrm{base}}} (J\sigma_f F^{-T})n_f \cdot e_1 \, \mathrm{d}s - \int_{\Gamma_i} (J\sigma_s F^{-T})n_s \cdot e_1 \, \mathrm{d}s$$

Further, using $\mathrm{div}(J\sigma_s F^{-T}) = 0$ since no right hand side is given in this benchmark configuration, the surface integral can be transformed into an integral over the complete circle Γ_{circle}:

$$J_{\mathrm{drag}}(U) = \int_{\Gamma_{\mathrm{circle}} \backslash \Gamma_{\mathrm{base}}} (J\sigma_f F^{-T})n_f \cdot e_1 \, \mathrm{d}s + \int_{\Gamma_{\mathrm{base}}} (J\sigma_s F^{-T})n_s \cdot e_1 \, \mathrm{d}s$$

An evaluation of this surface integral with higher accuracy is possible by expressing it in terms of residuals (the *Babuška-Miller-Trick*) [1, 2, 3, 21, 17] tested with a non-conforming test-function $\hat{Z}^{\mathrm{drag}} \notin X$

$$J_{\mathrm{drag}}(U) = A(U)(\hat{Z}^{\mathrm{drag}}), \quad \hat{Z}^{\mathrm{drag}} := \{0, 0, \hat{\chi}^u\}, \tag{18}$$

where

$$\hat{\chi}^u_y := 0, \quad \hat{\chi}^u_x := \left\{ \begin{array}{rl} 1 & : \; x \in \Gamma_{\mathrm{circle}} \\ \text{extended to } 0 & : \; x \notin \Gamma_{\mathrm{circle}} \cup \Gamma_{\mathrm{base}} \end{array} \right. .$$

Given sufficient regularity, the evaluation of the drag- and lift-coefficients using this technique yields a higher order of convergence [17], namely second order for linear finite elements. In the case of the lift-coefficients, the components $\hat{\chi}^u_y$ and $\hat{\chi}^u_x$ must be switched.

Obtaining Reference values of the FSI-1 benchmark problem. This benchmark problem is well analyzed in the collections [19, 20]. In Table 1 we collect reference values for all four functionals used in this work. These results are obtained by reviewing the cited references and extrapolating results using higher order finite elements on uniform meshes. The values are in very good agreement with those identified by Turek and coworkers [66].

functional	reference value	accuracy
drag	14.294	$\pm 5 \cdot 10^{-4}$
lift	0.7648	$\pm 5 \cdot 10^{-5}$
x-deformation	$2.268 \cdot 10^{-5}$	$\pm 5 \cdot 10^{-9}$
y-deformation	$8.190 \cdot 10^{-4}$	$\pm 5 \cdot 10^{-7}$

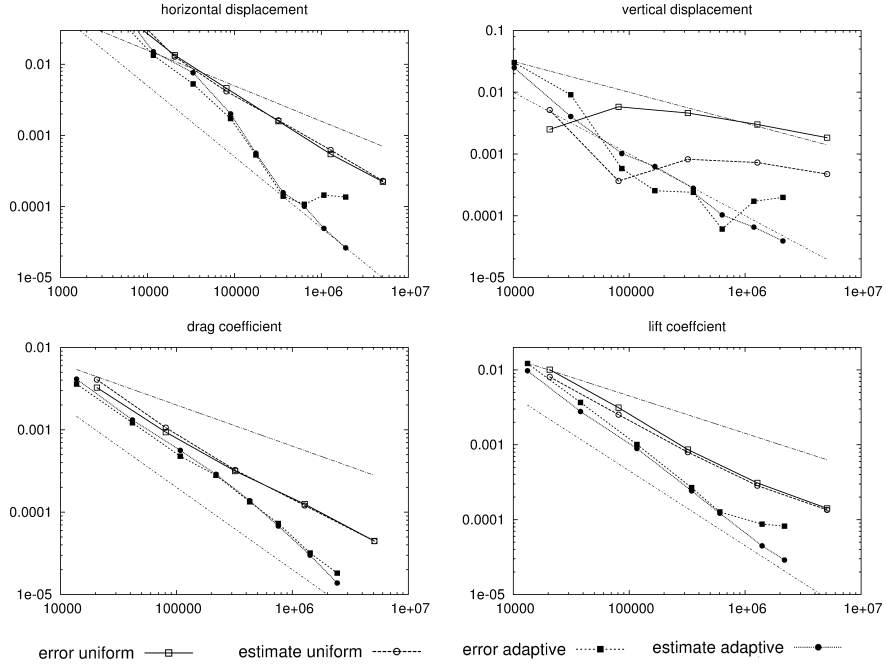Table 1: Reference values for the FSI-1 benchmark.

Figure 4: Error and estimator for the different functionals on uniform meshes and locally refined meshes. Top left to bottom right: error in horizontal and vertical deflection, drag- and lift-coefficient. For comparison: slopes with linear and quadratic convergence.

Error estimation and results on locally refined meshes. For error estimation with the dual weighted residual method we need to approximate the adjoint problems:

$$Z_h \in X_h : \quad A'_h(U_h)(\Phi_h, Z_h) = J'(U_h)(\Phi_h) \quad \forall \Phi_h \in X_h.$$

Detail on the adjoint bilinear-form are given in Section 5 and the appendix. For the two deflection functionals J_x, J_y, the right hand side of the adjoint problems is a Dirac and lacks the necessary regularity $J'_x, J'_y \notin H^{-1}(\Omega)$. Hence, these functionals should be regularized with a small parameter $\epsilon > 0$:

$$J_{x/y}(U) = \frac{1}{|B_\epsilon(A)|} \int_{B_\epsilon(A)} u_{x/y} \, \mathrm{d}x, \quad B_\epsilon(A) := \{x \in \Omega : |x - A| < \epsilon\}.$$

In the case of the drag- and lift-coefficients, the right hand side of the adjoint problems is defined by using $\hat{Z}^{\mathrm{drag}}$ from (18)

$$J'_{\mathrm{drag}}(U)(\Phi) = A'(U)(\Phi, \hat{Z}^{\mathrm{drag}}).$$

Since $\hat{Z}^{\mathrm{drag}}$ is a extension of (non-conforming) Dirichlet-values into the domain, this problem is related to solving a problem with homogenous right hand side
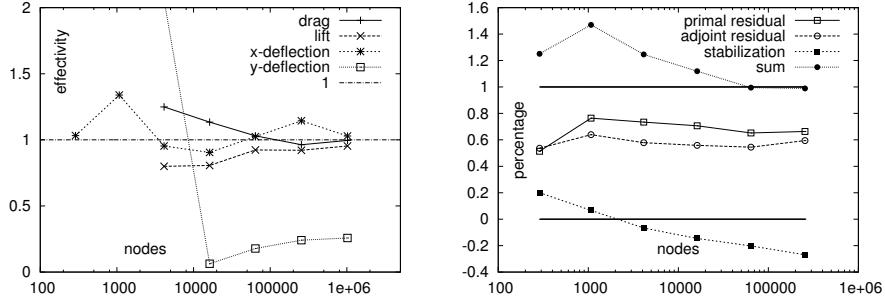
20

Figure 5: Effectivity of the dual weighted residual method on uniform meshes. Left: effectivities for all four functional values on uniform meshes. Right: composition of the estimator into primal residual, adjoint residual and stabilization part for the drag coefficient w.r.t the exact error.

and non-homogenous Dirichlet values on Γ_{circle}:

$$\hat{Z}_h \in \hat{Z}^{\text{drag}} + X_h : \quad A'_h(U_h)(\Phi_h, \hat{Z}_h) = 0 \quad \forall \Phi_h \in X_h.$$

In Figure 4, we compare the convergence history of all four error-functionals. In each sketch we compare the relative errors using uniform mesh refinement with those obtained on locally refined meshes using the dual weighted residual method. Further, on both sequences of meshes we plot the values of the error estimator. Finally, for comparison we give sketches of the error slopes corresponds to linear convergence $h \approx N^{-\frac{1}{2}}$ and quadratic convergence $h^2 \approx N^{-1}$. Note, that apparent loss of convergency on fine meshes (in particular for the lift-coefficient and the two displacement functionals) is due to limited accuracy of the reference values, see Table 1.

Next, in the left plot in Figure 5 we show the effectivities of the error estimator, namely

$$eff := \frac{\eta_h(U_h, Z_h)}{J(U) - J(U_h)},$$

on a sequence of uniform meshes for all four error functionals. A value of one indicates error estimation with optimal accuracy. In the right half of this Figure 5 we show the composition of the error estimator split into the primal residual $F(Z - i_h Z) - A_h(U_h)(Z - i_h Z)$, the adjoint residual $J'(U_h)(U - i_h U) - A'_h(U_h)(U - i_h U, Z_h)$ and the stabilization part $S_h(U_h)(Z_h)$ considering the drag-coefficient.

In Figure 6 we show the adjoint solutions with regard to the drag-evaluation. In the top-row the two components of the adjoint variable $w_f \in V_f$ which is only defined in Ω_f and in the bottom-row the two components of the variable $u \in V$ are shown. In the lower left plot one sees the Dirichlet-values $\hat{Z}^{\text{drag}}$ on the obstacle used to evaluate the drag coefficient.
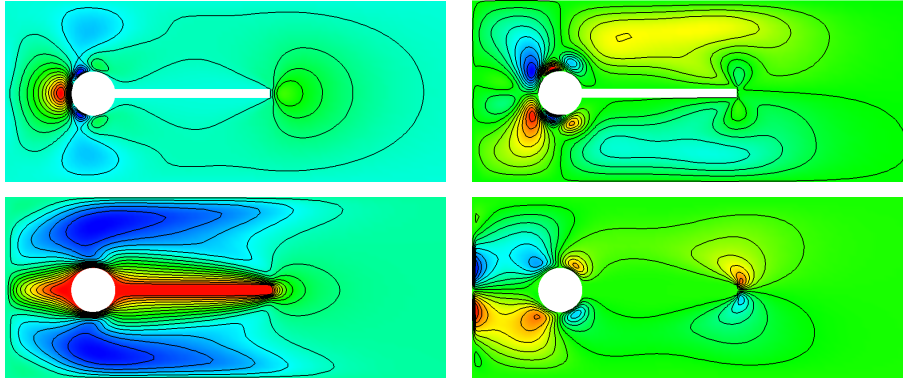
21

Figure 6: Adjoint solution with regard to the drag-coefficient. Top row: adjoint horizontal velocity w_f, bottom row, adjoint deformation z.

Discussion of the results. We start by discussing the results obtained on uniform meshes. Using piecewise linear finite elements, all four functionals should converge with second order (in the mesh size), given sufficient regularity of the solution. Figure 4 however depicts linear convergence only. This order reduction is due to limited regularity induced by the reentrant edges at the interface Γ_i as seen from the fluid domain. Similar results are observed for pure fluid dynamics benchmark problems [62, 17]. When comparing the estimator value with the real error in Figures 4 and 5, one observes very good effectivities $eff \xrightarrow[h \to 0]{} 1$ for the drag- and lift-coefficient (even if the regularity of the problem is not sufficient to guarantee higher order convergence of the remainders $\mathcal{R}^{(3)}$). In the case of the two deflection functionals - and in particular for the vertical deflection functional J_y - the quality of the estimator is less. This is explained by additional regularity limitations due to the Dirac structure of the functionals J_x and J_y.

The right sketch in Figure 5 shows that all three parts of the error estimator are essential. It is well known [10] that for linear problems primal and adjoint parts in the error estimator coincide (in the limit $h \to 0$). For nonlinear problems all parts must be taken into account. Further, we see that the stabilization part cannot be neglected. In Figure 7 we show some meshes with local mesh refinement obtained during the simulation.

6.2. 3D fluid-structure interaction

Problem configuration. Finally, we present numerical simulations of a three dimensional test-case. In the domain $\Omega := (0, 1.5) \times (0, 0.4) \times (-0.4, 0.4)$ an elastic structure $\Omega_s := (0.4, 0.5) \times (0, 0.2) \times (-0.2, 0.2)$ is inscribed, see Figure 8. The problem is considered to be symmetric in the x/y-plane. Hence, we run the simulation only in one half of the domain. On the inflow boundary $\Gamma_{\text{in}} = (0, 0.4) \times (-0.4, 0.4)$, a parabolic velocity profile is given as Dirichlet
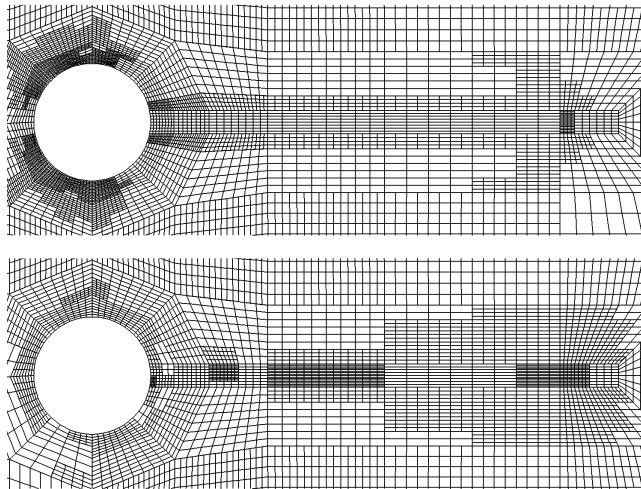
22

Figure 7: Cut-out of locally refined meshes used to approximate the drag-coefficient (top) and the horizontal displacement functional (bottom).

condition with peak velocity $v_{\max} = 0.3$. On the inner symmetry plane, we prescribe $v_f \cdot n = 0$ as Dirichlet condition, on the outflow boundary Γ_{out} the *do-nothing* condition for velocity and pressure. The no-slip condition is used on the remaining boundaries Γ_{wall}. The solid is fixed by a homogenous Dirichlet condition $u_s = 0$ on the bottom Γ_{base}. Deformation in normal-direction is prohibited $u_s \cdot n = 0$ on the symmetry-plane Γ_{sym}. On the remaining boundaries $\Gamma_{\text{wall}}, \Gamma_{\text{out}}$ and Γ_{in} the fluid's deformation is extended with homogenous Dirichlet values $u_f = 0$.

The fluid is incompressible with $\rho_f = 10^3$ and $\nu_f = 10^{-3}$. The solid's density is $\rho_s = 10^3$, its Poisson ratio $\nu_s = 0.4$ with a shear modulus of $\mu_s = 5 \cdot 10^5$. With an average inflow velocity of $\bar{v}_{\text{in}} \approx 0.15$, and an obstacle of size 0.2, the Reynolds number is $Re \approx 25$ and the flow is in the laminar regime. For the LPS stabilization, we set the parameter δ_0 in Problem 7 to the value $\delta_0 = 0.2$.

As quantities of interest, we measure the x-deflection of the obstacle at the coordinate $A = (0.45, 0.15, 0.15)$ close to the outer corner of the structure, as well as the force of the fluid on the structure in the dominant flow direction:

$$J_{\text{x}}(U) := e_1 \cdot u(A), \quad J_{\text{drag}}(U) := \int_{\Gamma_i} (J \sigma_f F^{-T}) n_f \cdot e_1 \, \mathrm{d}s.$$

Like in the two-dimensional case, the surface integral is first transformed using the structure equation and then expressed as a residual term $J_{\text{drag}}(U) = a(U)(\hat{Z}^{\text{drag}})$ using a function $\hat{Z}^{\text{drag}} \notin X$ with non-conforming boundary values at Γ_{base}, compare (18).

Obtaining Reference values of the 3d benchmark problem. For obtaining reference values we estimate the two error quantities on a sequence of meshes using
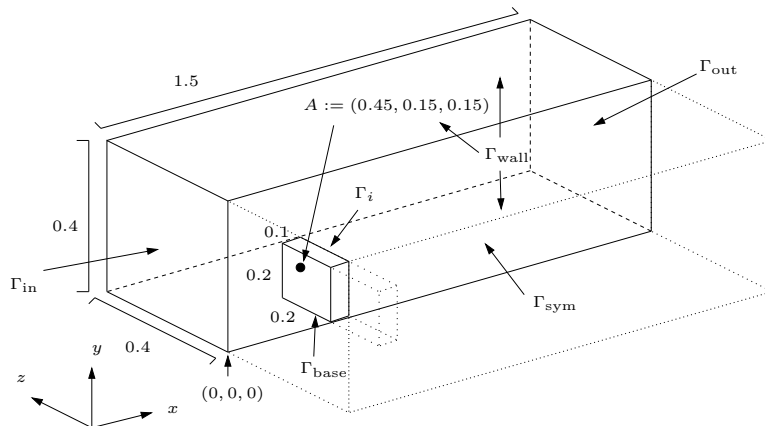
23

Figure 8: Configuration of the three-dimensional test-case. Domain and solution are symmetric in z-direction.

dof's	$J_{\mathrm{drag}}(U_h)$	error (abs)	$J_{\mathrm{x}}(U_h)$	error (abs)
2 975	1.5249	$1.98 \cdot 10^{-1}$	$4.9337 \cdot 10^{-5}$	$9.90 \cdot 10^{-6}$
18 711	1.4763	$1.49 \cdot 10^{-1}$	$5.5686 \cdot 10^{-5}$	$3.55 \cdot 10^{-6}$
131 495	1.4038	$7.68 \cdot 10^{-2}$	$5.8529 \cdot 10^{-5}$	$7.11 \cdot 10^{-7}$
983 367	1.3563	$2.93 \cdot 10^{-2}$	$\mathbf{5.9075 \cdot 10^{-5}}$	$\mathbf{1.65 \cdot 10^{-7}}$
7 600 775	**1.3380**	$\mathbf{1.10 \cdot 10^{-2}}$	$5.9202 \cdot 10^{-5}$	$3.80 \cdot 10^{-8}$

Table 2: Convergence history of the three dimensional fsi test-case using piecewise linear finite elements. The bold lines indicate, that an error below 1% has been reached.

uniform refinement. Table 2 we collect the results. By extrapolating, using the values on the finest three meshes, we define reference values in Table 3.

functional	reference value	accuracy
drag	1.33	1%
x-deflection	$5.95 \cdot 10^{-5}$	1%

Table 3: Reference values for the three dimensional benchmark problem.

We believe these values to be exact to a relative error of about 1%. Further refinements using parallel computers and higher order finite elements on adapted meshes are necessary to generate reference values with a higher accuracy. Here however we refrain from using higher order finite elements, since the reconstruction method for evaluating the error estimator in Section 5.4 would
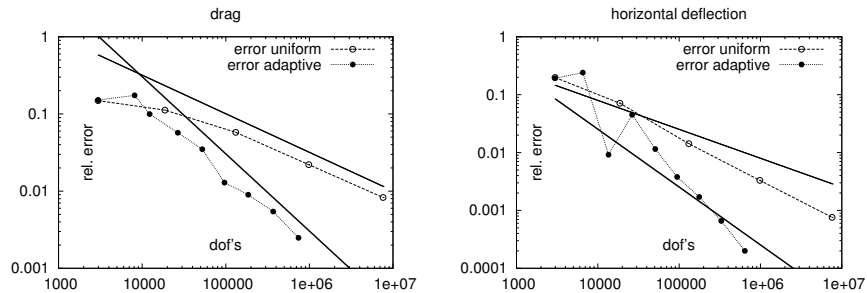
Figure 9: Error history for the drag-coefficient (left) and horizontal displacement (right) on uniform and adaptively refined meshes. Linear and quadratic error slopes for comparison.

require an even larger patch structures of the mesh which is not feasible without parallel computers.

Error estimation and results on locally refined meshes. In Figure 9 we plot the convergence history on uniform and locally refined meshes, both for the drag-coefficient and the horizontal displacement functional.

This three dimensional test-case has the same regularity limitations as the FSI-1 benchmark problem. The elastic obstacle induces corner singularities in the solution and the horizontal deflection functional J_x lacks regularity. In both cases, the computational effort necessary to reach a certain error tolerance is reduced significantly by using adaptive finite elements. Considering the complexity of three dimensional simulations these savings are substantial. In order to resolve the singularities caused by the reentrant corners of the embedded structure, it was essential to run the adaptation process very slowly by choosing $\alpha = 8$ in (17).

Finally, Figure 10 shows a visualization of a numerical solution. Here, adaptation is driven in order to optimize the functional value $J_x(U_h)$. Deformation of the structure is scaled by 100 for better visualization.

7. Conclusion

Focus of this work is the accurate analysis of a weak formulation used to derive methods for goal oriented error estimation of fluid-structure interaction problems. By completely mapping the problem onto the ALE reference system, the proper interface coupling condition is included in the variational formulation. This formulation is canonic in the sense, that the dual weighted residual error estimator is applicable in a straightforward way. At least for regular error functionals like the drag or lift coefficient, the proposed error estimator gives highly accurate estimates for the error. This result demonstrates the exactness of the linearized adjoints. These estimates can be used to generate efficient
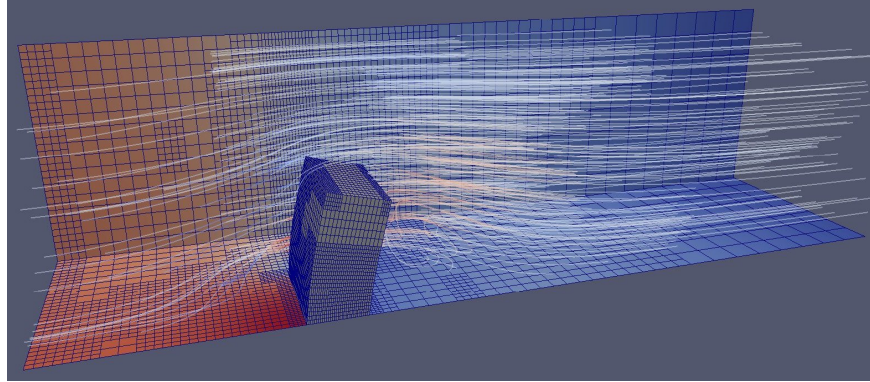
25

Figure 10: Sketch of the numerical solution on locally refined meshes. The domain is cut at the symmetry plane Γ_{sym} in the front.

meshes for obtaining functional values. In particular when dealing with complex three dimensional problems the possible saving due to accurate adaptive meshes are immense.

The variational formulation derived for goal-oriented error estimation has further impact on all numerical schemes where adjoint problems are involved. In particular, the correct representation of the adjoint interface coupling conditions is of importance when considering optimization of fluid-structure interaction problems. In further steps, in particular in the direction of hemodynamics applications, the variational formulation of the coupled problem as well as the adjoint formulation can be extended to more complex structure models [45] and also to non-Newtonian flow models [46]. Both issues add further nonlinearities to the formulation and will pose difficulties in the context of accurate error estimation.

A. Linearization of the fluid-structure interaction problem

The coupled fluid-structure interaction Problem 7 is given as:

$$U \in \tilde{U} + X : \quad A(U)(\Phi) = (J\rho_f f_f, \phi_f)_f + (\rho_s f_s, \phi_s)_s \quad \forall \Phi \in X',$$

where the semi-linear-form is defined by Problems 2 to 7:

$$A(U)(\Phi) := A_f(U)(\Phi) + A_s(U)(\Phi) + A_m(U)(\Phi) + S_h(U)(\Phi).$$

We need linearizations of this semi-linear-form for calculating the Jacobian in the Newton iteration

$$J(U)(W, \Phi) := A'_h(U)(W, \Phi) = \frac{d}{ds} A(U + sW)(\Phi)\Big|_{s=0}, \tag{19}$$

26

and to define the adjoint bilinear-form

$$A^*(Z, \Phi) := A'_h(U)(\Phi, Z) = \frac{d}{ds} A(U + s\Phi)(Z)\Big|_{s=0}. \tag{20}$$

As discussed, the Jacobian is the transpose of the adjoint system matrix. The derivatives are evaluated by successive execution of chain rule and product rule. Details on linearizations for a coupled fluid-structure interaction problem using similar structural models are found for instance in [34, 4]. A detailed analysis of the coupling of linear flow models with string-type solids is given in [72, 73].

A.1. Jacobian of the fluid-structure interaction problem

We start by giving a description of the Jacobian (19). Here, we use the notation:

$$U := \{u, v_f, p_f\} \in X, \quad \Phi := \{\phi, \psi_f, \xi_f\} \in X', \quad W := \{z, w_f, q_f\} \in X'.$$

First, we gather some basic definitions. For 2nd order tensors A, B, C it holds with $A : B = \sum_{ij} A_{ij} B_{ij}$:

$$AB : C = A : CB^T = B : A^T C, \quad \mathrm{tr}(A)I : B = A : \mathrm{tr}(B)I, \quad \mathrm{tr}(A^T B) = A : B \tag{21}$$

For a direction $z \in [H^1]^d$ it holds:

$$\frac{\partial F}{\partial u}(z) = \nabla z, \quad \frac{\partial F^T}{\partial u}(z) = \nabla z^T. \tag{22}$$

Following [45] we obtain the important results for the derivative of the inverse of the deformation gradient F^{-1} and its determinant J:

$$\frac{\partial F^{-1}}{\partial u}(z) = -F^{-1}\nabla z F^{-T}, \quad \frac{\partial J}{\partial u}(z) = J F^{-T} : \nabla z = J \mathrm{tr}(F^{-1}\nabla z) \tag{23}$$

In the following we discuss the derivatives of the three parts A_f, A_s and A_m separately.

The St. Venant Kirchhoff material. The semi-linear-form $A_s(\cdot)(\cdot)$ depends on the deformation u only. Therefore we only need to calculate the derivatives with respect this one variable. By relation (22) it holds for the Green-Lagrange strain tensor:

$$\frac{\partial E_s}{\partial u}(z) = \frac{1}{2}(\nabla z^T F + F^T \nabla z)$$

Thus:

$$\frac{\partial \Sigma_s}{\partial u}(z) = \frac{\lambda}{2} \mathrm{tr}\left(\nabla z^T F + F^T \nabla z\right) I + \mu_s(\nabla z^T F + F^T \nabla z),$$

and finally

$$A'_s(U)(W, \Phi) = \left(\nabla z \Sigma_s + F(\mu_s(\nabla z^T F + F^T \nabla z) + \lambda_s \mathrm{tr}(F^T \nabla z)I), \nabla \phi\right)_s. \tag{24}$$

Mesh motion problem. The variational formulation $A_m(\cdot)(\cdot)$ in Problem 5 is linear and depends on the fluid's deformation u_f only. The linearized form of the pseudo-elastic extension directly follows as:

$$A'_m(U)(W,\Phi) = \left(\mu_m(\nabla z + \nabla z^T) + \lambda_m \operatorname{div}(z), \nabla \psi_f\right)_f \tag{25}$$

In the case of a harmonic extension this simplifies to:

$$A'_m(U)(W,\Phi) := (\mu_m \nabla z, \nabla \psi_f)_f. \tag{26}$$

Navier-Stokes in ALE coordinates. The semi-linear-form $A_f(U)(\Phi)$ in Problem 4 depends on velocity, pressure and artificial deformation. We discuss the corresponding derivatives separately. The derivatives of the stress tensor with respect to pressure and velocity are given as:

$$\frac{\partial(J\sigma_f F^{-T})}{\partial v_f}(w_f) = J\rho_f \nu_f (\nabla w_f F^{-1} + F^{-T} \nabla w_f^T) F^{-T}$$

$$\frac{\partial(J\sigma_f F^{-T})}{\partial p_f}(q_f) = -Jq_f F^{-T}.$$

Together with the convective part we get:

$$\begin{aligned}
A'_{f,vp}(U)(W,\Phi) = & \left(J(\rho_f \nu_f(\nabla w_f F^{-1} + F^{-T} \nabla w_f^T) - q_f I)F^{-T}, \nabla \phi\right)_f \\
& + (\rho_f J F^{-1} v_f \cdot \nabla w_f, \phi)_f + (\rho_f J F^{-1} w_f \cdot \nabla v_f, \phi)_f \qquad (27) \\
& + (\operatorname{div}(J F^{-1} w_f), \xi_f)_f
\end{aligned}$$

It remains to gather all derivatives with respect to the artificial deformation of the fluid domain. By using relation (23) and with

$$\operatorname{div}(J F^{-1} v_f) = J \operatorname{tr}(F^{-1} \nabla v)$$

it holds that

$$\begin{aligned}
\frac{\partial(J \operatorname{tr}(F^{-1} \nabla v_f))}{\partial u}(z) &= J \operatorname{tr}(F^{-1} \nabla z) \operatorname{tr}(F^{-1} \nabla v_f) - J \operatorname{tr}(F^{-1} \nabla z F^{-1} \nabla v_f) \\
&= J F^{-1} \nabla z : F^{-1} \nabla v_f - J F^{-1} \nabla z F^{-1} \nabla v_f : I \\
&= J F^{-1} \nabla z : (F^{-1} \nabla v_f - \nabla v_f^T F^{-T})
\end{aligned}$$
$$\tag{28}$$

The derivatives of the convective term are

$$\frac{\partial(J F^{-1} v_f \cdot \nabla v_f)}{\partial u}(z) = J\left(\operatorname{tr}(F^{-1} \nabla z) F^{-1} - F^{-1} \nabla z F^{-1}\right) v_f \cdot \nabla v_f. \tag{29}$$

Finally, the derivatives of the stress tensor with respect to u are given by:

$$\frac{\partial(J\sigma_f F^{-T})}{\partial u}(z) = J\left(\operatorname{tr}(F^{-1} \nabla z)\sigma_f - \sigma_f F^{-T} \nabla z^T + \frac{\partial \sigma_f}{\partial u}(z)\right) F^{-T}, \tag{30}$$

with
$$\frac{\partial \sigma_f}{\partial u}(z) = -\rho_f \nu_f (\nabla v_f F^{-1} \nabla z F^{-1} + F^{-T} \nabla z^T F^{-T} \nabla v_f^T). \qquad (31)$$
Combining (28)-(31)

$$
\begin{aligned}
A'_{f,u}(U)(W, \Phi) = {}& (JF^{-1}\nabla z : (F^{-1}\nabla v_f - \nabla v_f^T F^{-T}), \xi_f)_f \\
& + \left(J\big(\operatorname{tr}(F^{-1}\nabla z)F^{-1} - F^{-1}\nabla z F^{-1}\big)v_f \cdot \nabla v_f, \phi\right)_f \\
& + \left(J\big(\operatorname{tr}(F^{-1}\nabla z)\sigma_f - \sigma_f F^{-T}\nabla z^T\big)F^{-T}, \nabla \phi\right)_f \\
& + -\rho_f \nu_f \big(J\nabla v_f F^{-1}\nabla z F^{-1} + F^{-T}\nabla z^T F^{-T}\nabla v_f^T, \nabla \phi\big)_f
\end{aligned}
\qquad (32)
$$

The Jacobian of the fluid-structure interaction problem is composed as:

$$
\begin{aligned}
A'(U)(W, \Phi) = {}& A'_s(U)(z, \phi) + A'_{f,u}(U)(z, \{\phi, \xi_f\}) \\
& + A'_m(U)(z, \psi_f) + A'_{f,vp}(U)(\{w_f, q_f\}, \{\phi, \xi_f\}),
\end{aligned}
\qquad (33)
$$

using the parts defined by (24), (25) or (26), (27) and (32).

A.2. Adjoint formulation of the fluid-structure interaction problem

The adjoint bilinear form formally follows by transposing the Jacobian:

$$A^*(Z, \Phi) := A'(U)(\Phi, Z),$$

where the adjoint solution $Z \in X$ is denoted by:

$$Z := \{z, w_f, q_f\} \in X.$$

The role of test- and trial space is switched:

$$\{z, w_f, q_f\} \leftrightarrow \{\phi, \psi_f, \xi_f\}.$$

Reviewing (33), the adjoint bilinear-form is given as:

$$
\begin{aligned}
A^*(Z, \Phi) := A'(U)(\Phi, Z) = {}& A'_s(U)(\phi, z) + A'_{f,u}(U)(\phi, \{z, q_f\}) \\
& + A'_m(U)(\phi, w_f) + A'_{f,vp}(U)(\{\psi_f, \xi_f\}, \{z, q_f\})
\end{aligned}
\qquad (34)
$$

The derivation of a strong formulation of this adjoint system can be done by tedious tensor analysis. However, for implementation and evaluation of the error estimator there is no need for this transformation, since the adjoint system matrix is assembled by transposing the Jacobian.

We want to stress the important role of switching test- and trial spaces. The *search direction z* in the Jacobian takes the role of the test-function ϕ in the adjoint problem. This test-function is defined globally on Ω and thus interface coupling terms appear on Γ_i due to integration by parts. Comparing (34), ϕ appears in the linearization of the structure problem A_s, the mesh motion problem A_m and the Navier-Stokes system A_f. All these terms give rise to a Neumann-type coupling condition on the interface between the adjoint variable

z on the solid domain and z, w_f and q_f on the fluid-domain. Further, w_f has trace zero on Γ_i. It holds:

$$\left.\begin{array}{r} w_f = 0 \\ S_s(z)n_s + S_f(Z, w_f, q_f)n_f = 0 \end{array}\right\} \text{ on } \Gamma_i.$$

By $S_s(\cdot)$ and $S_f(\cdot)$ we denote Neumann-type operators on the interface Γ_i.

References

[1] I. Babuška and A.D. Miller. The post-processing approach in the finite element method. I. calculations of displacements, stresses and other higher derivatives of the displacements. *Int. J. Numer. Meth. Engrg.*, 20:1085–1109, 1984.

[2] I. Babuška and A.D. Miller. The post-processing approach in the finite element method. II. the calculation of stress intensity factors. *Int. J. Numer. Meth. Engrg.*, 20:1111–1129, 1984.

[3] I. Babuška and A.D. Miller. The post-processing approach in the finite element method. III. a posteriori error estimation and adaptive mesh selection. *Int. J. Numer. Meth. Engrg.*, 20:2311–2324, 1984.

[4] Y. Bazilevs, V.M. Calo, T.J.R Hughes, and Y. Zhang. Isogeometric fluid-structure interaction: theory, algorithms, and computations. *Comput Mech*, 43:3–37, 2008.

[5] R. Becker and M. Braack. A finite element pressure gradient stabilization for the Stokes equations based on local projections. *Calcolo*, 38(4):173–199, 2001.

[6] R. Becker and M. Braack. A two-level stabilization scheme for the Navier-Stokes equations. In et. al. M. Feistauer, editor, *Numerical Mathematics and Advanced Applications, ENUMATH 2003*, pages 123–130. Springer, 2004.

[7] R. Becker, M. Braack, and R. Rannacher. Numerical simulation of laminar flames at low Mach number with adaptive finite elements. *Combust. Theory Modelling*, 3:503–534, 1999.

[8] R. Becker and R. Rannacher. Weighted a posteriori error control in FE methods. In et al. H. G. Bock, editor, *ENUMATH'97*. World Sci. Publ., Singapore, 1995.

[9] R. Becker and R. Rannacher. A feed-back approach to error control in finite element methods: Basic analysis and examples. *East-West J. Numer. Math.*, 4:237–264, 1996.

[10] R. Becker and R. Rannacher. An optimal control approach to a posteriori error estimation in finite element methods. In A. Iserles, editor, *Acta Numerica 2001*, volume 37, pages 1–225. Cambridge University Press, 2001.

[11] F. Bengzon and M.G. Larson. Adaptive finite element approximation of multiphysics problems: A fluid-structure interaction model problem. *Int. J. Numer. Methods. Eng*, 84:1451–1465, 2010.

[12] H. Blum. Asymptotic error expansion and defect correction in the finite element method. Habilitationsschrift, Institut für Angewandte Mathematik, Universität Heidelberg, 1991. SFB-123 Preprint 640.

[13] H. Blum, Q. Lin, and R. Rannacher. Asymptotic error expansion and richardson extrapolation for linear finite elements. *Numer. Math.*, 49:11–37, 1986.

[14] M. Braack, E. Burman, and N. Taschenberger. Duality based a posteriori error estimation for quasi-periodic solutions using time averages. *SIAM J. Sci. Comput.*, 33:2199–2216, 2011.

[15] M. Braack and A. Ern. Adaptive computation of reactive flows with local mesh refinement and model adaptation. In et. al. M. Feistauer, editor, *Numerical Mathematics and Advanced Applications, ENUMATH 2003*, pages 159–168. Springer, 2004.

[16] M. Braack and G. Lube. Finite elements with local projection stabilization for incompressible flow problems. *Journal of Computational Mathematics*, 27:116–147, 2009.

[17] M. Braack and T. Richter. Solutions of 3D Navier-Stokes benchmark problems with adaptive finite elements. *Computers and Fluids*, 35(4):372–392, May 2006.

[18] M. Braack and T. Richter. Stabilized finite elements for 3-d reactive flows. *Int. J. Numer. Meth. Fluids*, 51:981–999, 2006.

[19] H.-J. Bungartz and M. Schäfer, editors. *Fluid-Structure Interaction. Modelling, Simulation, Optimisation*, volume 53 of *Lecture Notes in Computational Science and Engineering*. Springer, 2006. ISBN-10: 3-540-34595-7.

[20] H.-J. Bungartz and M. Schäfer, editors. *Fluid-Structure Interaction II. Modelling, Simulation, Optimisation*. Lecture Notes in Computational Science and Engineering. Springer, 2010.

[21] G.F. Carey, S.S. Chow, and M.K. Seager. Approximate boundary-flux calculations. *Comp. Meth. Appl. Mech. Engrg*, 50:107–120, 1985.

[22] P.G. Ciarlet. *Finite Element Methods for Elliptic Problems*. North-Holland, Amsterdam, 1978.

[23] J. Donea. An arbitrary lagrangian-eulerian finite element method for transient dynamic fluid-structure interactions. *Comp. Meth. Appl. Mech. Eng.*, 33:689–723, 1982.

[24] T. Dunne. *Adaptive Finite Element Approximation of Fluid-Structure Interaction Based on Eulerian and Arbitrary Lagrangian-Eulerian Variational Formulations.* PhD thesis, University of Heidelberg, 2007. urn:nbn:de:bsz:16-opus-79448.

[25] T. Dunne, R. Rannacher, and T. Richter. Numerical simulation of fluid-structure interaction based on monolithic variational formulations. In G.P. Galdi and R. Rannacher, editors, *Comtemporary Challenges in Mathematical Fluid Mechanics.* World Scientific, Singapore, 2010.

[26] K. Eriksson, D. Estep, P. Hansbo, and C. Johnson. Introduction to adaptive methods for differential equations. In A. Iserles, editor, *Acta Numerica 1995*, pages 105–158. Cambridge University Press., 1995.

[27] K. Eriksson and C. Johnson. An adaptive finite element method for linear elliptic problems. *Math. Comp.*, 50(182):361–383, 1988.

[28] K. Eriksson and C. Johnson. Adaptive finite element methods for parabolic problems I: A linear model probelm. *SIAM J. Numer. Anal.*, 28(1):43–77, 1991.

[29] K. Eriksson and C. Johnson. Adaptive finite element methods for parabolic problems II: Optimal error estimates in $l_\infty l_2$ and $l_\infty l_\infty$. *SIAM J. Numer. Anal.*, 32(3):706–740, 1995.

[30] K. Eriksson and C. Johnson. Adaptive finite element methods for parabolic problems IV: Nonlinear problems. *SIAM J. Numer. Anal.*, 32(6):1729–1749, 1995.

[31] K. Eriksson and C. Johnson. Adaptive finite element methods for parabolic problems V: Lomg-time integration. *SIAM J. Numer. Anal.*, 32(6):1750–1763, 1995.

[32] D. Estep, V. Carey, V. Ginting, S. Tavener, and T. Wildey. A posteriori error analysis of multiscale operator decomposition methods for multiphysics models. *J. Phys: Conf. Series*, 125, 2008.

[33] M.A. Fernández and J.-F. Gerbeau. Algorithms for fluid-structure interaction problems. In L. Formaggia, A. Quarteroni, and A. Veneziani, editors, *Cardiovascular Mathematics: Modeling and simulation of the circulatory system*, volume 1 of *MS & A*, pages 307–346. Springer, 2009.

[34] M.A. Fernández and M. Moubachir. A newton method using exact jacobians for solving fluid-structure coupling. *Computers and Structures*, 83:127–142, 2005.

[35] P.W. Fick, E.H. van Brummelen, and K.G. van der Zee. On the adjoint-consistent formulation of interface conditions in goal-oriented error estimation and adaptivity for fluid-structure interaction. *Computer Methods in Applied Mechanics and Engineering*, 199:3369–3385, 2010.

[36] Luca Formaggia and Fabio Nobile. A stability analysis for the arbitrary Lagrangian Eulerian formulation with finite elements. *East-West Journal of Numerical Mathematics*, 7:105 – 132, 1999.

[37] Luca Formaggia, Alfio Quarteroni, and Alessandro Veneziani. *Cardiovascular Mathematics: Modeling and simulation of the circulatory system*. Springer-Verlag, Italia, Milano, 2009.

[38] O. Ghattas and X. Li. A variational finite element method for stationary nonlinear fluid-solid interaction. *Journal of Computational Physics*, 121:347–356, 1995.

[39] M.B. Giles and E. Süli. Adjoint methods for pdes: a posteriori error analysis and postprocessing by duality. *Acta Numerica 2002*, pages 145–236, 2002. A. Iserles, ed.

[40] T. Grätsch and K.J. Bathe. Goal-oriented error estimation in the analysis of fluid flows with structural interactions. *Computer Methods in Applied Mechanics and Engineering*, 2006:5673–5684, 195.

[41] Ralf Hartmann. Multitarget error estimation and adaptivity in aerodynamic flow simulations. *SIAM J. Sci. Comput.*, 31(1):708–731, 2008.

[42] M. Heil, A.L. Hazel, and J. Boyle. Solvers for large-displacement fluid-structure interaction problems: Segregated vs. monolithic approaches. *Computational Mechanics*, 43, 2008.

[43] B.T. Helenbrook. Mesh deformation using the biharmonic operator. *Int. J. Numer. Meth. Engrg.*, pages 1–30, 2001.

[44] J.G. Heywood, R. Rannacher, and S. Turek. Artificial boundaries and flux and pressure conditions for the incompressible Navier-Stokes equations. *Int. J. Numer. Math. Fluids*, 22:325–352, 1992.

[45] G.A. Holzapfel. *Nonlinear Solid Mechanics: A Continuum Approach for Engineering*. Wiley-Blackwell, 2000.

[46] J. Hron and S. Turek. A monolithic fem/multigrid solver for an ale formulation of fluid-structure interaction with applications in biomechanics. In H.-J. Bungartz and M. Schäfer, editors, *Fluid-Structure Interaction: Modeling, Simulation, Optimization*, Lecture Notes in Computational Science and Engineering, pages 146–170. Springer, 2006.

[47] J. Hron, S. Turek, M. Madlik, M. Razzaq, H. Wobker, and J.F. Acker. Numerical simulation and benchmarking of a monolithic multigrid solver for fluid-structure interaction problems with application to hemodynamics. In H.-J. Bungartz and M. Schäfer, editors, *Fluid-Structure Interaction II: Modeling, Simulation, Optimization*, Lecture Notes in Computational Science and Engineering, pages 197–220. Springer, 2010.

[48] A. Huerta and W.K. Liu. Viscous flow with large free-surface motion. *Computer Methods in Applied Mechanics and Engineering*, 69(3):277–324, 1988.

[49] T.J.R. Hughes and A.N. Brooks. Streamline upwind Petrov Galerkin formulations for convection dominated flows with particular emphasis on the incompressible Navier-Stokes equation. *Computer Methods in Applied Mechanics and Engineering*, 32:199–259, 1982.

[50] T.J.R. Hughes, L.P. Franca, and M. Balestra. A new finite element formulation for computational fluid dynamics: V. circumvent the Babuska-Brezzi condition: A stable Petrov-Galerkin formulation for the Stokes problem accommodating equal order interpolation. *Computer Methods in Applied Mechanics and Engineering*, 59:89–99, 1986.

[51] T.J.R. Hughes, W.K. Liu, and T.K. Zimmermann. Lagrangian-eulerian finite element formulations for incompressible viscous flows. *Computer Methods in Applied Mechanics and Engineering*, 29:329–349, 1981.

[52] A.A. Johnson and T.E. Tezduyar. Mech update strategies in parallel finite element computations of flow problems with moving boundaries and interfaces. *Comput. Meth. Appl. Mech. Eng.*, 119:73–94, 1994.

[53] A.A. Johnson and T.E. Tezduyar. Advanced mesh generation and update methods for 3d flow simulations. *Comp. Mech.*, 23:130–141, 1999.

[54] M.G. Larson and A. Målqvist. Goal oriented adaptivity for coupeld flow and transport problems with applications in oil reservoir simulation. *Comput. Meth. Appl. Mech. Eng.*, 196:3546–3561, 2007.

[55] P. Le Tallec and J. Mouro. Fluid structure interaction with large structural displacement. *Comp. Meth. Appl. Mech. Engrg*, 190:3039–3067, 2001.

[56] H.G. Matthies and J. Steindorf. Partitioned but strongly coupled iteration schemes for nonlinear fluid-structure interactions. *Comp. Struct.*, 80:1991–1999, 2002.

[57] H.G. Matthies and J. Steindorf. Partitioned strong coupling algorithms for fluid-structure interaction. *Comp. Struct.*, 81:805–812, 2003.

[58] J.T. Oden and S. Prudhomme. On goal-oriented error estimation for elliptic problems: Application to the control of pointwise errors. *Comput. Methods Appl. Mech. Engrg.*, 176:313–331, 1999.

[59] M. Paraschivoiu and A.T. Patera. Hierarchical duality approach to bounds for the outputs of partial differential equations. *Comput. Methods Appl. Mech. Engrg.*, 158:389–407, 1998.

[60] R. Rannacher and F.-T. Suttmeier. A feed-back approach to error control in finite element methods: Application to linear elasticity. *Computer Methods in Applied Mechanics and Engineering*, 19:434–446, 1997.

[61] T. Richter. A posteriori error estimation and anisotropy detection with the dual weighted residual method. *Int. J. Numer. Meth. Fluids*, 62(1):90–118, 2010.

[62] M. Schäfer and S. Turek. Benchmark computations of laminar flow around a cylinder. (With support by F. Durst, E. Krause and R. Rannacher). In E.H. Hirschel, editor, *Flow Simulation with High-Performance Computers II. DFG priority research program results 1993-1995*, number 52 in Notes Numer. Fluid Mech., pages 547–566. Vieweg, Wiesbaden, 1996.

[63] J. Sokołowski and J.-P. Zolésio. *Introduction to shape optimization*, volume 16 of *Computational Mathematics*. Springer, 1992.

[64] K. Stein, T.E. Tezduyar, and R. Benney. Automatic mesh update with solid-extension mesh moving technique. *Comp. Meth. Appl. Mech. Eng.*, 193:2019–2032, 2004.

[65] T.E. Tezduyar. Finite element methods for fluid dynamics with moving boundaries and interfaces. *Arch. Comput. Methods. Eng.*, 8:83–130, 2001.

[66] S. Turek, J. Hron, M. Razzaq, H. Wobker, and M. Sch"afer. Numerical benchmarking of fluid-structure interaction: A comparison of different discretization and solution approaches. In H.J. Bungartz, M. Mehl, and M. Schäfer, editors, *Fluid Structure Interaction II: Modeling, Simulation and Optimization*. Springer, 2010.

[67] W.A. Wall. *Fluid-Structure Interaction with Stabilized Finite Elements*. PhD thesis, University of Stuttgart, 1999. urn:nbn:de:bsz:93-opus-6234.

[68] T. Wick. Fluid-structure interactions using different mesh motion techniques. *Computers and Structures*, 89:1456–1467, 2011.

[69] J. Wloka. *Partielle Differentialgleichungen*. Teubner, Stuttgart, 1982.

[70] K.G. van der Zee, E.H. van Brummelen, I. Akkerman, and R. de Borst. Goal-oriented error estimation and adaptivity for fluid-structure interaction using exact linearized adjoints. *Comput. Methods Appl. Mech. Engrg.*, 200:2738–2757, 2011.

[71] K.G. van der Zee, E.H. van Brummelen, and R. de Borst. Goal-oriented error estimation for stokes flow interacting with a flexible channel. *Int. J. Numer. Meth. Fluids*, 56:1551–1557, 2008.

[72] K.G. van der Zee, E.H. van Brummelen, and R. de Borst. Goal-oriented error estimation and adaptivity for free-boundary problems: The domain-map linearization approach. *SIAM J. on Scientific Computing*, 32(2):1074 – 1092, 2010.

[73] K.G. van der Zee, E.H. van Brummelen, and R. de Borst. Goal-oriented error estimation and adaptivity for free-boundary problems: The shape-linearization approach. *SIAM J. on Scientific Computing*, 32(2):1093–1118, 2010.